BULGARIAN ACADEMY OF SCIENCES
STEFAN ANGELOV INSTITUTE OF MICROBIOLOGY

SIMEON EMILOV DIMITROV

Evaluation of the Potential of New Derivatives of Ethambutol and Isoniazid for the Study of Their Antitubercular Activity

ABSTRACT

of PhD thesis in a professional direction 4.3. Biological Sciences, Scientific specialty "Microbiology"

Scientific Supervisors:
Assoc. Prof. Violeta Valcheva Ruseva, PhD
Prof. Milka Milcheva Mileva, PhD

Scientific jury:
Assoc. Prof. Maya Zacharieva, PhD
Prof. Stefan Panayotov, DSc, PhD
Assoc. Prof. Neli Vilhelmova-Ilieva, PhD
Assoc. Prof. Lyubomira Yocheva, PhD
Assoc. Prof. Denitsa Stefanova, PhD

БЪЛГАРСКА АКАДЕМИЯ на НАУКИТЕ 1869

Sofia, 2025

The dissertation comprises 154 pages, including 40 figures and 20 Tables

s. The bibliography cites 346 literary sources. The experimental work was conducted at the Mycobacterial Molecular Biology Laboratory of the Stephan Angeloff Institute of Microbiology, Bulgarian Academy of Sciences (BAS).

The dissertation was reviewed and approved for public defense on …… 2025 during an extended meeting of the National Seminar on Infectious Microbiology at the Stephan Angeloff Institute of Microbiology – BAS. The public defense will be held before a scientific jury on …… at …… in the conference hall of the Stephan Angeloff Institute of Microbiology – BAS. The defense materials are available at the office of the Scientific Secretary of The Stephan Angeloff Institute of Microbiology – BAS.

CONTENTS

List of Abbreviations

BDQ	Bedaquiline
COVID-19	Coronavirus Disease 2019
EMB	Ethambutol
GPx	Glutathione Peroxidase
GSH	Glutathione
i.p.	Intraperitoneally
INH	Isoniazid
InhA	Enoyl-Reductase
KatG	Catalase-Peroxidase
LJ	Löwenstein-Jensen Medium
M7H9	Middlebrook 7H9 Medium
M7H10	Middlebrook 7H10 Medium
MDA	Malondialdehyde
MDR-TB	Multidrug-Resistant Tuberculosis
MIC	Minimum Inhibitory Concentration
ADR	Adverse Drug Reactions
OS	Oxidative Stress
p.o.	Per os (Orally)
RIF	Rifampicin
ROS	Reactive Oxygen Species
SOD	Superoxide Dismutase
WHO	Whole-Genome Sequencing
WGS	Bedaquiline

I. INTRODUCTION

Tuberculosis remains a serious public health issue despite advances in combating infectious diseases. The disease is difficult to control and poses challenges to researchers and clinicians. Although drugs, vaccines, and preventive measures are available, effective outcomes are often hindered by various factors. According to the WHO, the COVID-19 pandemic has worsened the situation, leading to an increase in undiagnosed and untreated cases, which are major sources of transmission and carry a higher risk of complications and mortality.

The most serious problems in tuberculosis control is the development of drug resistance, especially multidrug resistance. This is defined as resistance of *Mycobacterium tuberculosis* to the two most effective anti-tuberculosis drugs, rifampicin and isoniazid, simultaneously. In the early 21st century, the first cases of extensively drug-resistant tuberculosis were reported, characterized by resistance to several antibiotics, and prevalent in regions such as Africa, Asia, and some Eastern European countries.

COVID-19, the global economic downturn, and increased migration have complicated the situation, with the rise in the number of migrants, homeless people, and individuals dependent on alcohol and drugs leading to higher tuberculosis incidence and increased drug resistance. This creates favorable conditions for the selection of spontaneous mutations causing resistance to various anti-tuberculosis drugs.

To control the global tuberculosis epidemic, there is an urgent need to develop new anti-tuberculosis agents that reduce treatment time and effectively target MDR/XDR strains at low doses. Recent scientific data summarize new synthetic compounds with high *in vitro* activity against *Mycobacterium tuberculosis* H37Rv, often exceeding that of standard drugs.

However, many of these fail in preclinical and clinical trials due to toxicity, poor bioavailability, or pharmacokinetic issues. The main requirements for new compounds are high antimycobacterial activity, low toxicity, and minimal risk of adverse effects. Therefore, the focus of the present study was on the biological and pharmacological screening of newly synthesized substances to evaluate their efficacy and mechanisms of action against various strains of *Mycobacterium tuberculosis.*

II. AIM AND OBJECTIVES

The aim of this dissertation is to conduct a pharmacological screening of pre-selected newly synthesized chemical compounds with respect to their antimycobacterial activity and toxicity, as well as to clarify certain aspects of their mechanism of action against *Mycobacterium tuberculosis*.

1. In accordance with this goal, the experimental work was directed toward the execution of the following tasks;
2. To determine the *in vitro* antimycobacterial activity of the newly synthesized chemical compounds against reference strains *Mycobacterium tuberculosis* H37Rv and Mycobacterium smegmatis MC2155;
3. To analyze the energetic interactions between protein targets of *M. tuberculosis* and the synthesized compounds, and to identify molecules (ligands) with high affinity for these targets using molecular docking;
4. To investigate the transmembrane permeability of selected compounds.
5. To assess the *in vitro* cytotoxicity and in vivo acute and subacute toxicity in a mouse experimental model, as well as to monitor histopathological changes and markers of oxidative damage in target organs;
6. To investigate the redox-modulating capacity of the compounds in chemical model systems;
7. To induce *in vitro* mutagenesis and isolate DNA from resistant mutants, followed by whole genome sequencing and bioinformatic analysis.

III. MATERIALS AND METHODS

III.1. MATERIALS

1. Newly Synthesized Compounds

The compounds selected for this dissertation were chosen based on their high *in vitro* antitubercular activity, previously studied by the Laboratory of Mycobacterial Molecular Biology at the Stephan Angeloff Institute of Microbiology, BAS. These include newly synthesized aroylhydrazones from the Department of Chemistry at the Medical University – Sofia and nitrofuranilamides from the Institute of Organic Chemistry with Centre of Phytochemistry at BAS.

2. Bacterial Strains

The reference strains used were Mycobacterium smegmatis MC2 155 — a fast-growing, non-pathogenic model, provided by the Federal Research and Clinical Center of Physical-Chemical Medicine in Moscow and maintained at the "Stephan Angeloff" Institute of Microbiology, BAS. The strain *Mycobacterium tuberculosis* H37Rv (ATCC 25618) was provided with the assistance of the Research Institute of Phthisiopulmonology in Saint Petersburg, Russia.

3. Culture Media

Selective media used for culturing mycobacteria included: Löwenstein-Jensen (LJ); Middlebrook 7H10 agar (M7H10); Middlebrook 7H9 broth (M7H9).

4. Cell Lines

Several cell lines were used: HEK293 (human embryonic kidney epithelial cells), CCL-1 (transformed mouse fibroblasts), HeLa (human cervical tumor cell line), MIA PaCa (human pancreatic tumor cell line), HepG2 (liver tumor cells), WA13 (human fibroblasts), KMST (human tumor cells), and WI-38 (human lung fibroblasts), in accordance with ISO 10993-5:2009 standard for biocompatibility.

5. Experimental Animals

Male and female mice from the Jcl:ICR strain, aged 6 weeks and weighing between 25 and 30 g, were used.

All experiments were conducted in accordance with the principles of the European Convention for the Protection of Vertebrate Animals Used for Experimental and Other Scientific Purposes (ETS 123), with measures taken to minimize animal suffering.

III.2. METHODS

1. Determination of Antitubercular Activity

The minimum inhibitory concentration (MIC) was determined using the REMA method (Martin et al., 2012).

2. *In Vitro* Cytotoxicity

The cytotoxic activity of the tested compounds was assessed using the standard colorimetric MTT assay (3-(4,5-dimethylthiazol-2-yl)-2,5-diphenyltetrazolium bromide).

3. Molecular Docking

The software Molecular Operating Environment (MOE, 2022) was used for molecular modeling and docking analysis with four crystallographic protein structures of *M. tuberculosis:* InhA with ligands TCU (PDB: 2X22) and 641 (PDB: 4TZK), GlfT2 (PDB: 4FIY), and oxidoreductase (PDB: 4NXI).

4. Determination of Transmembrane Permeability of Active Compounds

The PAMPA (Parallel Artificial Membrane Permeability Assay) method was used to predict passive membrane permeability, following the Double-Sink™ protocol using artificial membranes mimicking the gastrointestinal tract and blood-brain barrier.

5. *In Vivo* Determination of Acute and Subacute Toxicity

Studies were conducted in accordance with OECD guidelines (2001) and ISO 10993-2/12 standards. Acute toxicity was determined using a modified Lorke method.

6. Histopathological Evaluation of Tissue Samples

Histopathological evaluation of liver, kidneys, and small intestines from experimental mice was performed using the classical histological method described by Lillie (1964).

7. Antioxidant Activity and Redox-Modulating Capacity

7.1. Determination of Total Protein in Liver Homogenate

Total protein content was measured using the Biuret method with a ready-made kit from Cromatest/Lineal Chemicals (REF 1153020).

7.2. Determination of Total Glutathione (tGSH) in Liver Homogenate

Total glutathione content was quantified using the method by Rahman et al. (2005).

7.3. Determination of Glutathione Peroxidase and Glutathione Reductase Activity

The activity of glutathione peroxidase (GPx) and glutathione reductase (GRd) was tested using commercial kits (REF CGP1 and GRSA) and measured spectrophotometrically.

7.4. Determination of Malondialdehyde (MDA) – a marker of lipid peroxidation

MDA levels were measured using the Hunter method, adapted by Mileva et al. (2000), as a marker of oxidative stress.

7.5. Enzymatic Activity of Superoxide Dismutase (SOD)

SOD activity was determined using the method by Beauchamp and Fridovich (1971).

7.6. Investigation of *In Vitro* Antioxidant Capacity

7.6.1. DPPH Assay

The method by Brand-Williams (1995) was used to evaluate antioxidant activity.

7.6.2. ABTS Assay

Antioxidant activity was assessed using the ABTS method (Re et al., 1999; adapted by Erel, 2005). Results were compared to the activity of Trolox and expressed as Trolox equivalents.

8. *In Vitro* Mutagenesis and DNA Isolation from Resistant Mutants

8.1. *In Vitro* Mutagenesis

A bacterial suspension of M. smegmatis MC2155 or *M. tuberculosis* H37Rv was standardized to 1 McFarland (3.0 × 10^8 CFU/ml) and plated on agar.

8.2. Isolation of Chromosomal DNA from Resistant Mutants

Chromosomal DNA isolation from resistant mutants was performed using the method of van Embden (1993).

8.3. Whole Genome Sequencing and Data Analysis

The whole genome sequencing was conducted using the Illumina HiSeq platform, and the genome data were deposited in the NCBI Sequence Read Archive.

IV. RESULTS AND DISCUSSION

1. Synthesis of Selected and Novel Chemical Compounds — Analogues of INH and EMB

Series of aroylhydrazone derivatives (analogues of isoniazid, INH) (Figure 1) and nitrofuranilamides (derivatives of ethambutol, EMB) were synthesized and purified. The chemical structures were confirmed using NMR spectroscopy, mass spectrometry, and physicochemical characterization methods (Figures 2 and 3). The introduction of protective groups into the hydrazide–hydrazone system proved to be an effective strategy for preventing enzymatic inactivation and the formation of toxic metabolites. The aroylhydrazones exhibited selective antimycobacterial activity and showed potential for FabH inhibition, as supported by QSAR (Quantitative Structure–Activity Relationship) analysis.

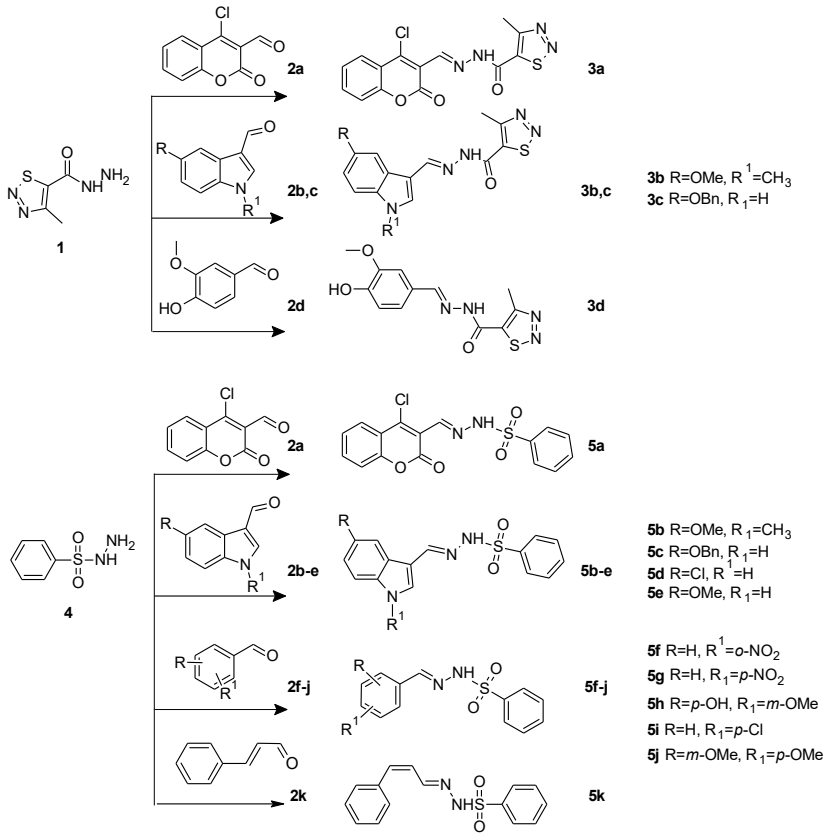

Figure 1. Synthesis and chemical structure of the aroylhydrazone series.

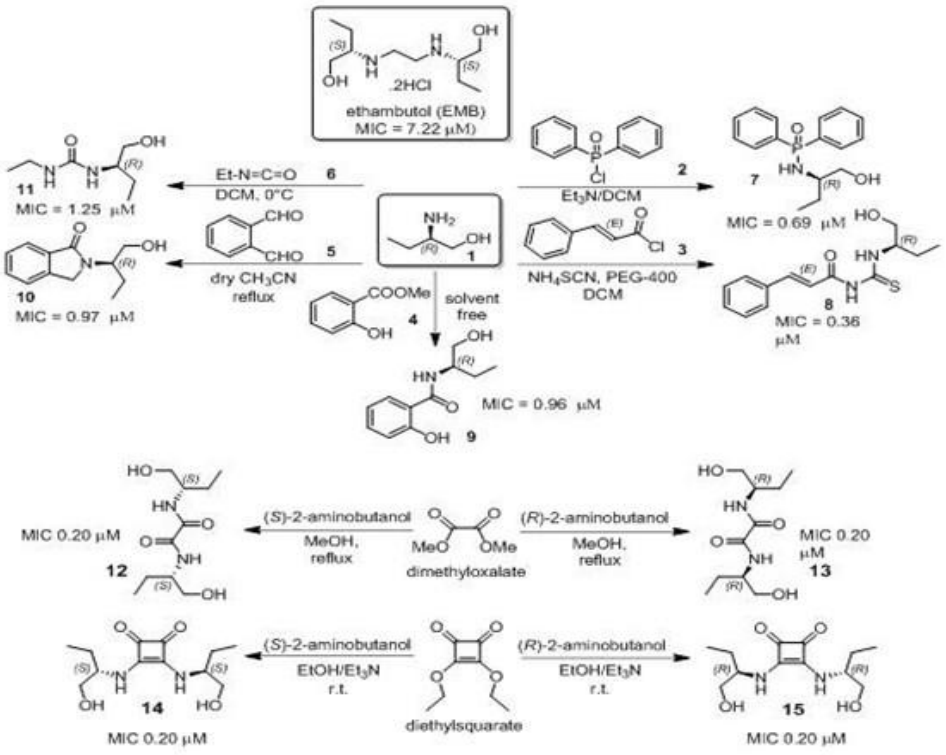

Figure 2. Synthesis and chemical structure of the nitrofuranilamide series (1–15).

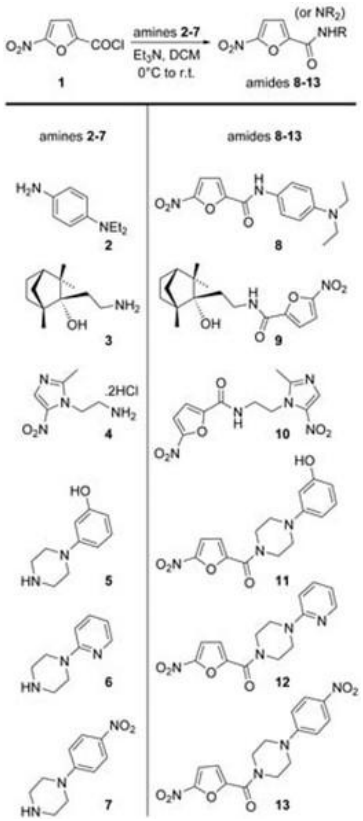

Figure 3. Synthesis and chemical structure of the nitrofuranilamide series (2–13).

The mechanism of action of nitrofuranylamides involves the reduction of the nitro group by enzymes called nitroreductases, which are localized in the bacterial cell wall. This process leads to the formation of free radicals that damage cellular components and cause the elimination of pathogens (Krasavin et al., 2018). According to Wang et al., the enzyme deazaflavin F420-dependent nitroreductase (Ddn) is the main catalyst for the activation of the nitrofuran JSF-2019. Similarly, the nitro group in nitroimidazole drugs such as pretomanid and delamanid undergoes intracellular metabolism mediated by the same enzyme. In *M. tuberculosis*, Ddn performs a function analogous to that of NsfA/NsfB in E. coli (Jian, Y. et al., 2021).

2. *In vitro* antimycobacterial activity of aroylhydrazones and nitrofuranylamides

Aroylhydrazones (3a–3d), sulfonylhydrazones (5a–5k), and nitrofuranylamides (8–13) were investigated. Among them, compound 3a showed the highest activity, with values below 0.08 µM. The inclusion of a sulfonylhydrazone fragment (e.g., in 5c) led to reduced activity compared to their aroylhydrazone analogs (3c). Compound 3d, containing a 5-benzyloxyindole scaffold, also demonstrated significant activity (MIC = 0.4412 µM). This confirms the relationship between structure and biological activity (Viveiros, 2012; Gupta et al., 2010).

The *in vitro* antimycobacterial activity of nitrofuranylamides confirmed their high efficacy (Table 2). Results from repeated experimental studies using the REMA method supported the selection of compounds 11, 12 (DO-190), and 13 (DO-209). Compound DO-190 demonstrated exceptionally promising results with an MIC of 0.20 μM, comparable to values observed for INH.

Table 1. MIC values determined by the REMA method

Compounds *	**MIC (μM)**
3a	0.0730
3b	0.3294
3c	0.1744
3d	0.4412
5a	0.1814
5d	0.1669
5b	0.2027
5c	0.3434
5e	0.1647
5f	0.1473
5g	0.3053
5h	0.0716
5i	0.0763
5j	0.3203
5k	0.3210
INH	0.0343

The chemical structures are presented in Figure 1.

Table 2. MIC values determined by the REMA method

Compounds *	**MIC (μM)**
8	16.48
9	29.73
10	16.2
11	0.50
12(DO190)	0.20
13(DO209)	0.36

The chemical structures are presented in Figure 2-3.

The nitrofuranilamides also exhibited high activity against M. *tuberculosis H37Rv* and *M. smegmatis*, likely due to efficient reduction of the nitro group (Foo et al., 2016), without loss of activity. The data are consistent with findings by Krasavin et al. (2019) and Jin-Bo et al. (2015), highlighting the broad-spectrum activity of nitrofurans. Comparison with the reference antibiotic rifampicin (RIF) shows that some of the tested compounds demonstrate comparable or even superior activity, confirming their potential as future therapeutic alternatives (Cho et al., 2007; Nandikolla et al., 2021). Structural optimization could further improve their pharmacological profile.

3. *In vitro* Cytotoxicity of Aroylhydrazones and Nitrofuranilamides

The *in vitro* cytotoxicity of the newly synthesized aroylhydrazones was evaluated on CCL-1 and HEK293 cell lines following treatment with selected compounds at concentrations ranging from 12.5 to 200 μM (Table 3). Aroylhydrazone compounds 3a–d, 5g, and 5k demonstrated excellent biocompatibility and selectivity, with a Selectivity Index (SI) > 1000. The most active were compounds 3a and 3d, exhibiting MIC values of 0.07 μM and low cytotoxicity (IC_{50} values of 256.7 μM and 217.5 μM, respectively). Notably, 3a outperformed established antitubercular drugs in terms of toxicological profile.
The comparison between 3a and 3d highlights the importance of the 1,2,3-thiadiazole fragment, as 3d was shown to be twice as effective as INH and four times more effective than ethambutol. These findings support the conclusion that structural modification is crucial for enhancing antimycobacterial activity and selectivity (Liu et al., 2024; Sruthi et al., 2022).
According to Bashir et al. (2023), the specific structure of the aroylhydrazone complex is responsible for cytotoxic activity against A549 cells.
The cytotoxicity of nitrofuranilamides 11, 12 (DO190), and 13 (DO209) was also *assessed in vitro* on various cell lines. Cells were treated with compounds at concentrations ranging from 1 to 100 μM. Results indicated that the compounds exhibited low cytotoxicity, showing no significant impact on cell viability regardless of cell line origin or characteristics (Figure 4).
Compounds DO190 and DO209 demonstrated minimal cytotoxicity after 24-hour treatment, with only a slight increase observed at prolonged exposure and high concentration (100 μM).

Table 3. Cytotoxicity of newly synthesized aroylhydrazones on HEK-293 and CCL-1 cell lines.

Compounds *	IC_{50} (µM) CCL-1	IC_{50} (µM) HEK	SI CCL-1	SI HEK
3a	256.7 ± 13.3	217.5 ± 17.2	3516	2979
3b	818.3 ± 23.7	361 ± 11.3	2487	1244
3c	390.8 ± 12.0	713.5 ± 18.5	2242	4093
3d	279.5 ± 42.5	217.5 ± 17.2	633	620
5a	48.0 ± 5.9	83.9 ± 4.0	267	463
5d	13.8 ± 0.9	16.9 ± 3.4	11	97
5b	2.9 ± 0.3	16.2 ± 2.7	14	82
5c	321.4 ± 16.2	32.3 ± 1.5	945	95
5e	5.1 ± 1.1	15.6 ± 4.1	31	95
5f	131.4 ± 11.4	100.1 ± 9.3	892	679
5g	72.4 ± 5.8	100.1 ± 2.1	237	327
5h	240 ± 9.6	158.5 ± 11.2	3380	2216
5i	191 ± 13.2	138.3 ± 7.4	1812	1819
5j	223 ± 11.5	150.2 ± 5.1	469	696
5k	83.5 ± 7.0	47.4 ± 6.8	146	260
INH	-	-	-	-

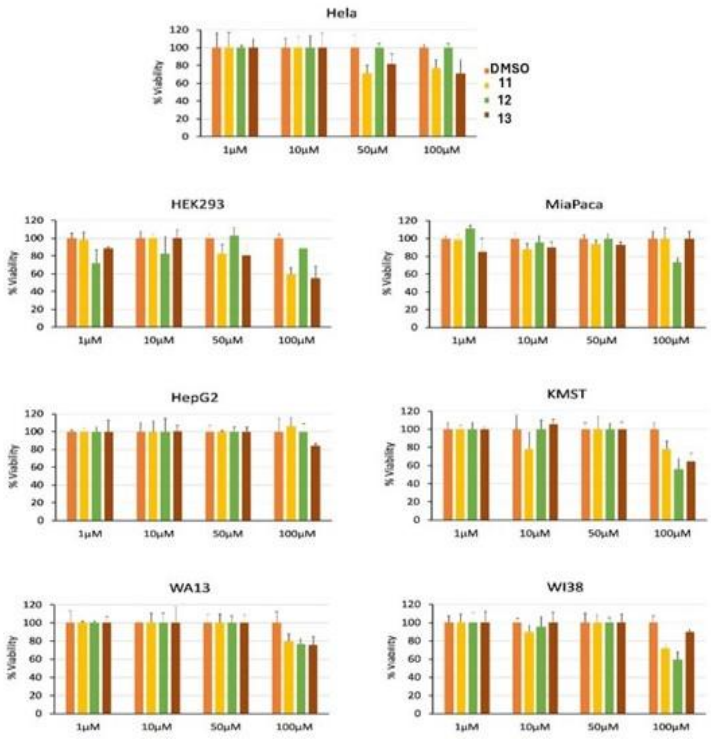

Figure 4. Evaluation of cell viability after treatment with nitrofuranilamides DO190 and DO209 in the concentration range of 1–100 µM.

4. Molecular Docking of Aroylhydrazones and Nitrofuranilamides. Determination of Transmembrane Permeability

Docking analyses revealed that the studied compounds exhibit significant affinity toward InhA, with binding free energies ranging from –12.36 to –10.02 kcal/mol for the 2X22 structure and from –14.67 to –11.10 kcal/mol for 4TZK (Table 4). The most active compounds based on minimal inhibitory concentration (MIC) 5k, 3a, and 3d — also rank among the top in docking affinity for 2X22. This suggests the presence of stable binding within the enzyme's active site and highlights their potential as candidates for the development of novel antimycobacterial agents.

Table 4. Docking results of the synthesized compounds with the 2X22 and 4TZK structures

Compounds	2X22* (kcal/mol)	4TZK* (kcal/mol)
3a	-10.93 (13)	-11.56 (14)
3b	-11.02 (15)	-12.38 (15)
3c	-11.09 (9)	-11.62 (13)
3d	-10 .02 (2)	-14,67 (6)
5a	-11.06 (10)	-12.15 (9)
5d	-10.99 (12)	-12.30 (7)
5b	-10.73 (14)	-12.66 (4)
5c	-11.60 (5)	-12.19 (8)
5e	-12.03 (3)	-14.67 (1)
5f	-11.29 (7)	-11.88 (10)
5g	-11.98 (4)	-12.80 (3)
5h	-11.43 (6)	-12.49 (5)
5i	-11.18 (8)	-11.87 (11)
5j	-11.06 (11)	-11.75 (12)
5k	-12.36 (1)	-12.83 (2)
INH	-9.18 (16)-	-8.51 (16)

* E_score1 – binding free energy from the first scoring stage, in kcal/mol;

** The chemical structures are presented in Figure 1.

Docking analysis with the 4TZK structure shows that compounds 5e and 3d exhibit the highest affinity (–14.67 kcal/mol), followed by 5k and 5g (–12.83 and –12.80 kcal/mol, respectively). The active compound 3a has a score of –12.38 kcal/mol, ranking sixth. In comparison, isoniazid (INH) demonstrates significantly weaker binding energy (–9.18

kcal/mol for 2X22 and –8.51 kcal/mol for 4TZK), confirming the higher inhibitory potential of the novel compounds toward the InhA enzyme. Figure 5 (A and B) presents the interactions between the ligand and InhA from *M. tuberculosis* (PDB: 2X22 and 4TZK), visualized using "Ligand Interactions" in MOE. The binding of co-crystallized ligands — TCU and 641 — to the ligand-binding domains of both receptors is illustrated.

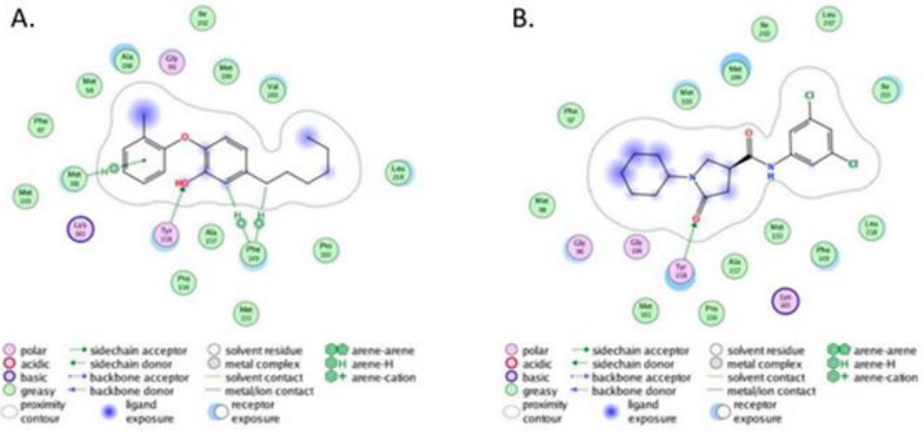

Figure 5. Interaction diagrams of the ligand-binding domains of *M. tuberculosis* InhA with: (A) 5-hexyl-2-(2-methylphenoxy) phenol (TCU) (PDB ID: 2X22) and (B) (3S)-1-cyclohexyl-N-(3,5-dichlorophenyl)-5-oxo pyrrolidine-3-carboxamide (641) (PDB ID: 4TZK).

Docking analyses of INH derivatives indicate that hydrogen bonds with Tyr158 and Ile194 are key for binding to InhA, consistent with literature data that also highlight Ser94, Gly96, Lys165, and Ile194. The interactions involve Phe149, Tyr158, and Met161, where Phe149 and Met161 form π–H (arene–hydrogen) bonds, and Tyr158 forms a hydrogen bond. Other residues (e.g., Gly96, Met199, Leu218) are located near the ligand but do not participate directly in interactions (see Figure 5B).

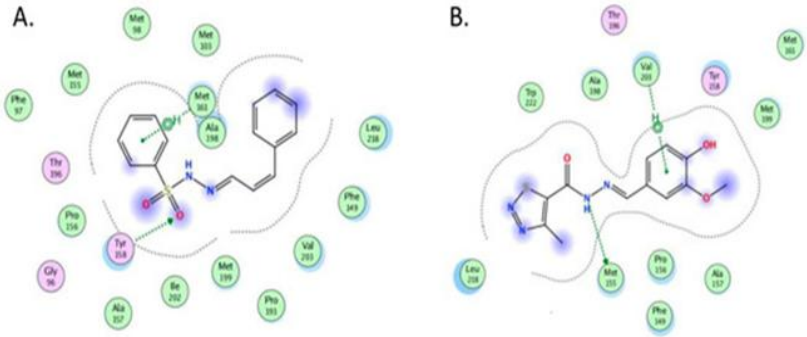

Figure 6. Interaction diagrams of the ligand-binding domain of M. tuberculosis InhA (2X22) with the most active compounds and top-scoring poses of (A) 5k and (B) 3a.

Figure 6 shows the protein-ligand interaction (PLI) diagrams for the most active compounds 5k and 3a, which exhibited the highest affinity scores in the docking analysis against the 2X22 receptor. As seen in Figure 6A, compound 5k, with the highest docking score, reproduces two key interactions in the active site of InhA — with Tyr158 and Met161. Compound 3a (Figure 6B) also demonstrates high activity but does not interact with Tyr158; instead, it forms a bond with Met155 and a π–H interaction with Val203. Compound 5e, despite a good docking score, only forms a single π–H interaction with Phe97.

Figure 7 summarizes the interaction profiles of the three top-ranked compounds — 5e, 5k, and 3a — presented through PLI (protein-ligand interaction) diagrams. These visualizations illustrate the spatial positioning of the compounds within the active site and their respective contact points with amino acid residues.

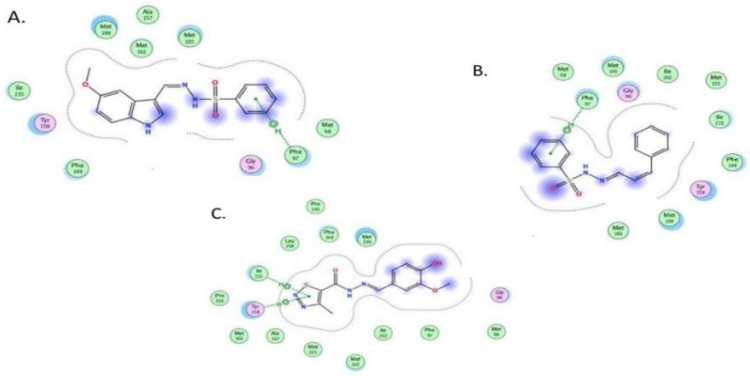

Figure 7. Interaction diagrams of the ligand-binding domains of *M. tuberculosis* InhA (4TZK) with the top-scoring compounds (A) 5e, (B) 5k, and (C) 3a.

Molecular docking showed that compounds 5e and 5k do not interact with Tyr158, suggesting an alternative binding mechanism. In contrast, compound 3a restores the π–H interaction with Tyr158 and forms a bond with Ile215, typical of the classical binding model.

All synthesized compounds bound to the ligand-binding domains of InhA are shown in Figure 8A (receptor 2X22) and Figure 8B (receptor 4TZK) using the Connolly surface representation. Docking of DO-190, DO-209, and EMB to four targets demonstrated that EMB occupies the most favorable position in three of them. INH and EMB were included as reference antitubercular agents (Tables 5 and 6).

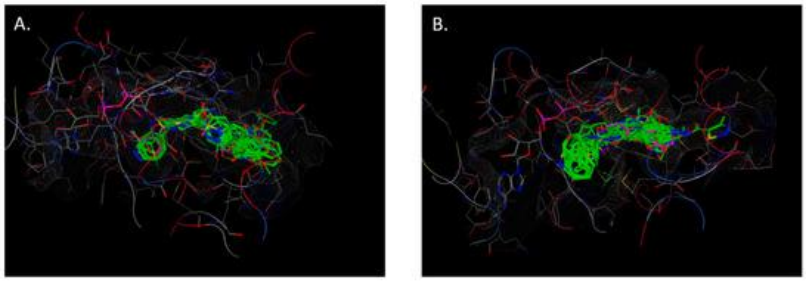

Figure 8. Docking conformations of all synthesized compounds (in green), ligands TCU (A) (in magenta) and 641 (B) (in magenta), and the corresponding Connolly surface.

Table 5. Docking results of the studied compounds in the active sites of InhA (PDB ID 2X22 and 4TZK), GlfT2 (PDB ID 4FIY), and oxidoreductase (PDB ID 4NXI).

Compounds	2X22* (kcal/mol)	4TZK* (kcal/mol)	4FIY* (kcal/mol)	4NXI* (kcal/mol)
DO-190	−11.65	−11.73	−9.20	−7.81
DO-209	−11.77	−11.67	−8.50	−6.73
EMB	−9.63	−10.73	−8.75	−8.45
INH	−9.69	−9.70)	−7.79	−8.90

*E_score 1 — free binding energy from the initial refinement step, in kcal/mol.

Nitroferricyanides DO-190 and DO-209 exhibit lower binding energies than EMB in the active sites of InhA (2X22, 4TZK). At GlfT2 (4FIY), their results are comparable, whereas for the oxidoreductase (4NXI), EMB outperforms both compounds. Compared to INH, DO-190 and DO-209 demonstrate better affinity for three out of the four targets. A PLI (protein-ligand interaction) analysis of the interactions between the compounds and the target proteins was also performed.

Table 6. Protein-ligand interaction (PLI).

Compounds	2X22	4TZK	4FIY	4NXI
DO-190	Phe149; Met199	Met199	Arg37	Asn41; Gly160
DO-209	Met155; Gly160	Tyr158	Glu30	Gln7; Asn41; Gly160
EMB	Tyr158; Met199; Glu30	Met199	Leu28; Glu30	Asp12

The molecular docking results reveal that DO-190 exhibits better binding energies than DO-209 in three out of four targets, except for InhA (2X22). EMB demonstrates hydrogen bonds with Tyr158 and Met199, while DO-190 reproduces the interaction with Met199 and forms a new arene–arene interaction with Phe149. DO-209 replicates the hydrogen bond with Tyr158 and establishes a new bond with Met155.

The coumarin, hydrazone, and pyrazole-conjugated coumarin structures prove to be key for binding to InhA, highlighting the importance of these fragments in inhibiting the bacterial cell wall. The synergy between these groups contributes to the potential overcoming of drug resistance.

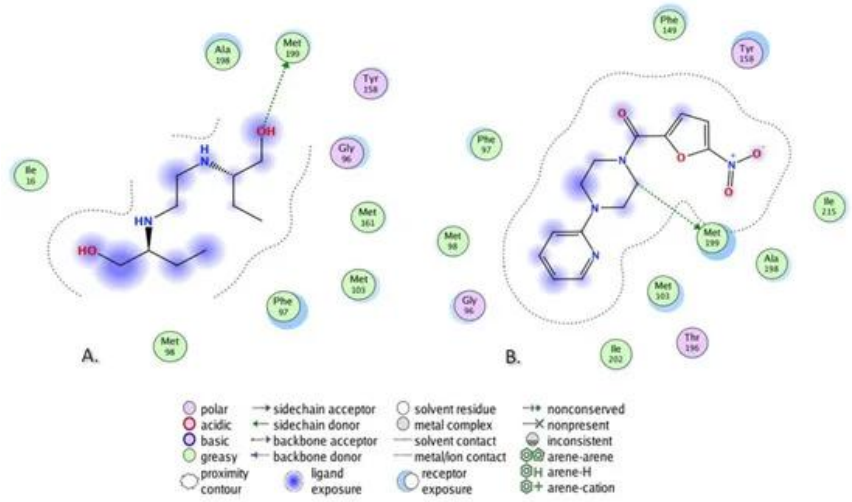

Figure 9. Docking conformations of INH (a), DO-190 (b), and DO-209 (c) in the ligand-binding domain of InhA (PDB ID 4TZK).

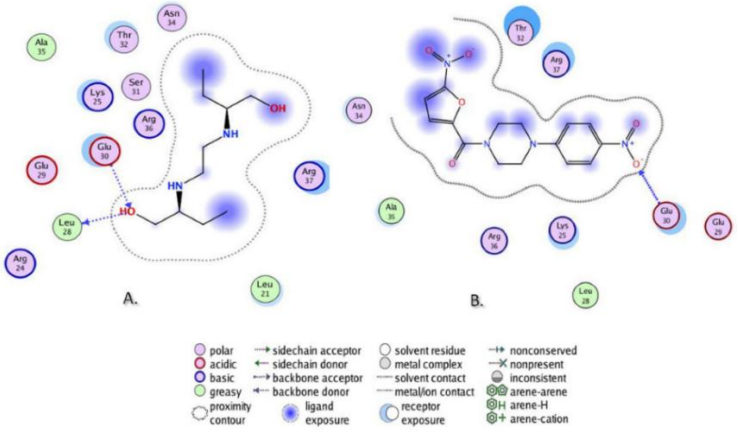

Figure 10. Docking conformations of DO-190 (a) and DO-209 (b) in the ligand-binding domain of GlfT2 (PDB ID 4FIY).

Analysis of interactions with GlfT2 (PDB ID 4FIY) showed no protein-ligand interactions (Figure 20). The compound DO-190 forms three key interactions: arene–H bonds with Glu30 and Arg36, as well as a hydrogen bond with Arg37. DO-209 replicates the arene–H interaction with Glu30.

For oxidoreductase (PDB ID 4NXI), none of the compounds reproduce the hydrogen bond with Asp12 characteristic of EMB, but both reveal new interactions with Asn41 and Gly160, while DO-209 additionally forms an interaction with Gly7. Asp12 is close to the ligand

but outside the binding range. The analysis indicates that DO-190 and DO-209 replicate some of the key interactions of EMB in three out of the four targets.

PAMPA results show that INH is impermeable under the given experimental conditions (–logPe > 6). The newly synthesized aroylhydrazone compounds exhibit significantly lower –logPe values (by 1–2 orders of magnitude) compared to INH (Table 7), indicating increased permeability.

Table 7. Gastrointestinal Permeability of INH and Its Newly Synthesized Derivatives

	-logPe, GIT PAMPA		
Compounds	pH=5	pH=6.2	pH=7.4
INH	6.226	6.591	6.594
3a	4.354	4.366	4.299
3d	4.158	4.137	4.150

GIT—gastrointestinal tract

Compounds 3a and 3d are classified as highly permeable across the tested pH range. The data also shows that changes in pH do not cause noticeable alterations in the permeability of the compounds. This suggests a pH-independent mechanism of penetration through the gastrointestinal tract membranes, which is theoretically supported by the physicochemical properties of the compounds. Therefore, PAMPA represents a rapid and well-established *in vitro* model for assessing the permeability of lipophilic compounds across various biological barriers, while minimizing the need for cellular assays or animal models (Bennion et al., 2017; Dahlgren et al., 2019; Fedi et al., 2021).

5. *In Vivo* Determination of Acute and Subacute Toxicity of Aroylhydrazones (3a and 3d) and Nitrofuranylamides (DO-190 and DO-209)

The acute toxicity of the aroylhydrazone compounds 3a and 3d was evaluated *in vivo* using 36 female mice via oral (p.o.) and intraperitoneal (i.p.) administration. The dosing ranges and observed clinical symptoms are summarized in Tables 8 and 9.

Table 8. Acute Intraperitoneal Toxicity of 3a in Female Mice.

Dose (mg/kg)	Effect Mortality	Time of onset	Symptoms
3000	2/3 (67%)	After 20 hours	Respiratory failure with long pauses, ataxia, piloerection, convulsions, lethal outcome
2000	1/3 (33%)	After 24 hours	Impaired coordination, lethal outcome
1500	1/3 (33%)	After 30 hours	Delayed reflexes, drowsiness, lethal outcome
1000	0/3	-	-
500	0/3	-	-

$LD50 = \sqrt{D0\ x\ D100}$ = $\sqrt{1000 \text{ x } 1500}$ = 1224,7 mg/ kg indicating that the LD_{50} for intraperitoneal (i.p.) administration is > 2000 mg/kg. For oral administration, no mortality was observed at the highest dose tested (3000 mg/kg), indicating that the LD_{50} for oral administration is > 2500 mg/kg.

The Index of Relative Toxicity (IR) was calculated as:. IR = (LD_{50} i.p. / LD_{50} p.o.) × 100 = (1225 / 2500) × 100 ≈ 49%. This value indicates that the absorption rate of the compound after oral administration is significantly lower compared to intraperitoneal administration (Table 8).

Table 9. Acute Intraperitoneal Toxicity of 3d in Female Mice.

Dose (mg/kg)	Effect Mortality	Time of onset	Symptoms
3000	1/3	After 3 hours	Impaired coordination, rapid breathing, clonic seizure, death
2000	0/3	-	-
1500	0/3	-	-
1000	0/3	-	-
500	0/3	-	-

$LD50 = \sqrt{\text{D0 x D100}}$ = $\sqrt{2000 \text{ x } 3000}$ = 2449.49, LD_{50} > 2000 mg/ kg or intraperitoneal (i.p.) administration, no mortality was observed at the highest oral dose of 3000 mg/kg, indicating that the LD_{50} for oral administration is >2500 mg/kg. IR = LD50 i.p. / LD50 p.os. x 100 = 489,89 / 692,82 x 100 ≈ 70,7%. Doses for subacute (14-day) oral exposure were determined based on the LD_{50} value, using the following fractions: 1/10 LD_{50} (250 mg/kg) and 1/20 LD_{50} (125 mg/kg) (see Table 9).

The acute toxicity of the nitrofuranylamides DO-190 and DO-209 was evaluated in 48 female mice after both oral and intraperitoneal administration. The dosage and observed clinical symptoms are summarized in Tables 10, 11, and 12.

Table 10. Acute Intraperitoneal Toxicity of DO-190 in Female Mice.

Dose (mg/kg)	Effect Mortality	Time of onset	Symptoms
3000	1/3	After 5 hours	Difficulty breathing, ataxia, slowed movements, isolation
2000	0/3	-	-
1500	0/3	-	-
1000	0/3	-	-
500	0/3	-	-

$LD50 = \sqrt{D0 \times D100} = \sqrt{2000 \times 3000} = 2449.49$, $LD_{50} > 2000$ mg/ kg, $LD_{50} > 2000$ mg/ kg For intraperitoneal (i.p.) administration. At the highest oral dose of 3000 mg/kg, no mortality was observed, indicating that the LD_{50} for oral (p.o.) administration is > 2500 mg/kg.

IR = LD50 i.p. / LD50 p.o. * 100 (%) = 2450/ 3000 x 100 ≈ 81,6 %

For subacute 14-day oral treatment, doses of 1/10 LD_{50} (250 mg/kg) and 1/20 LD_{50} (125 mg/kg) were used to evaluate the long-term tolerability of the compound (see Table 10).

Table 11. Acute oral toxicity of DO 190 in female mice.

Dose (mg/kg)	Effect Mortality	Time of onset	Symptoms
1000	3/3	15–30 min	Rapid breathing, ataxia, piloerection
800	2/3	After 0.5 hour	Difficulty breathing, ataxia
600	1/3	After 1 hour	Difficulty breathing, ataxia
400	0/3	-	-
200	0/3	-	-

$LD50 = \sqrt{D0 \times D100} = \sqrt{600 \times 400} = 489{,}89$; $LD_{50} \approx 500$ mg/ kg For i.p. administration, the LD_{50} value is approximately 500 mg/kg. This indicates that the compound exhibits relatively moderate toxicity via this route of administration (see Table 11).

Table 11. Acute oral toxicity of DO 209 in female mice.

Dose (mg/kg)	Effect Mortality	Time of onset	Symptoms
1000	2/3	After 15–30 min	Rapid breathing, impaired gait, clonic seizure, death
800	1/3	After 2 hours	Difficulty breathing, ataxia, hypoactivity
600	0/3	-	-
400	0/3	-	-
200	0/3	-	-

$LD50 = \sqrt{D0 \times D100} = \sqrt{800 \times 600} = 692{,}82$; $LD_{50} \approx 700$ mg/ kg, ко This yields a value of approximately 700 mg/kg for i.p. administration.

IR = LD50 i.p. / LD50 p.o. * 100 (%) = 489,89 /692,82 x 100 ≈ 70,7%. This indicates that the absorption of the compound via intravenous administration is approximately 70.7% of that observed with oral administration (Tables 12).

For the 14-day subacute oral treatment, doses corresponding to 1/10 (70 mg/kg) and 1/20 (35 mg/kg) of the LD_{50} were used to evaluate the compound's tolerance during prolonged exposure.

Following acute toxicity tests and a 14-day observation period, compounds 3a and 3d demonstrated good tolerance and no significant toxicological effects. Toxicity was slightly

increased with parenteral administration, but both compounds fall into the "slightly toxic" category according to the Hodge and Sterner classification, making them suitable for further investigation. In comparison, DO-190 was found to be significantly more toxic than DO-209, which is classified as a safer candidate.

During the 14-day observation period after acute toxicity testing, no behavioral abnormalities, physical condition changes, or neurotoxic symptoms were observed in the surviving animals. Food and water intake remained unchanged.

On day 14, the animals were humanely euthanized in accordance with ethical standards.

The subacute toxicity of derivatives 3a and 3d was evaluated in 36 male mice during a 14-day oral treatment. Body weight was measured throughout the period, and the results showed a significant increase at all dose levels (Figures 11 and 12).

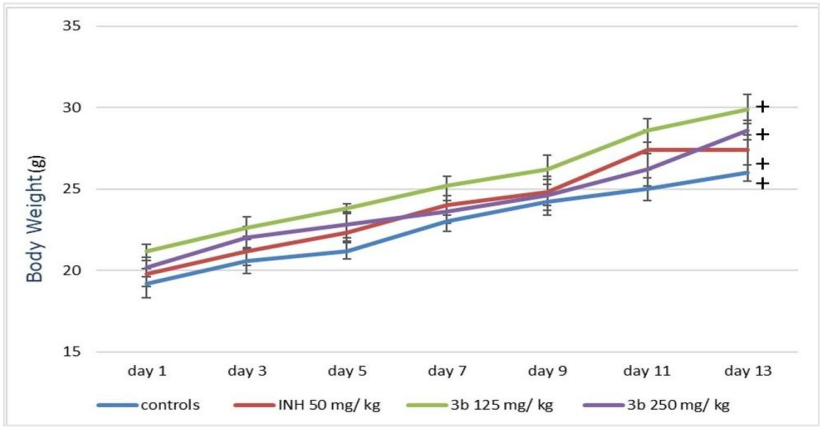

Figure 11. Changes in body weight of male mice treated with INH and 3a; +p < 0.05 compared to day 1 of the experimental period.

The highest increase was observed at 125 mg/kg – 41% for 3a and 44% for 3d compared to baseline values, confirming the absence of toxicity.

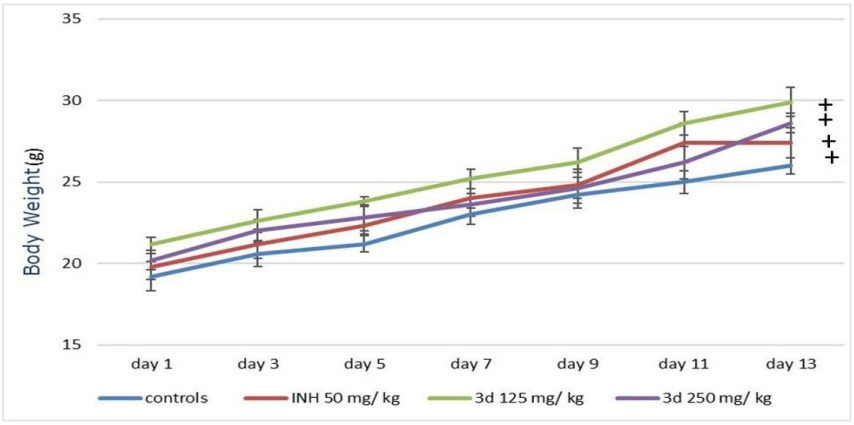

Figure 12. Changes in body weight of male mice treated with INH and 3d; +p < 0.05 compared to day 1 of the experimental period.

The subacute toxicity of compounds DO-190 and DO-209 was assessed after a 14-day oral exposure. Body weight was measured at the same time points, and the results are presented in Figures 13 and 14.

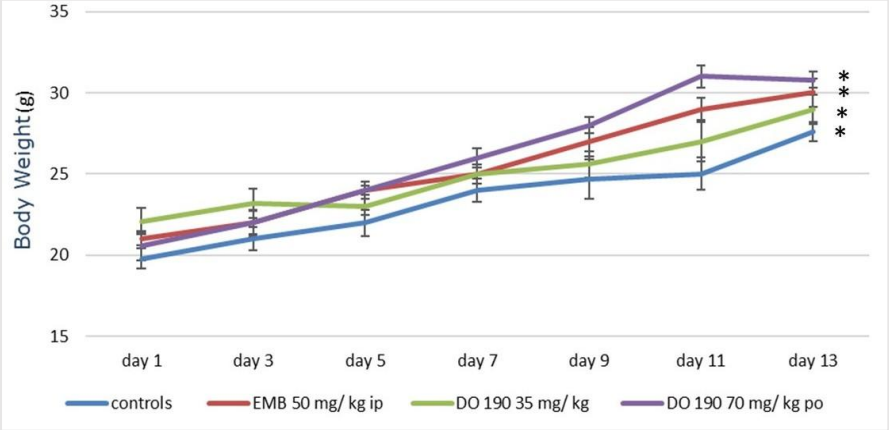

Figure 13. Changes in body weight of male mice treated with EMB and DO-190; $p < 0.05$ compared to day 1 of the experimental period.

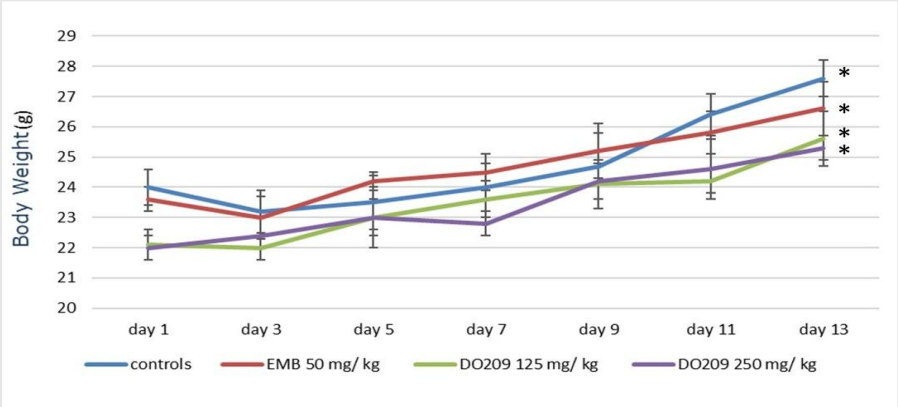

Figure 14. Changes in body weight of male mice treated with EMB and DO-209; $p < 0.05$ compared to day 1 of the experimental period.

On day 14 of the experiment, all surviving animals were euthanized in accordance with ethical protocols. Blood was collected for complete blood count (CBC) and biochemical analysis.

All experimental groups demonstrated an increase in body weight, with the most pronounced gain observed in animals treated with DO-190 at a dose of 70 mg/kg. By the end of the experimental period, the group receiving DO-190 (70 mg/kg) showed a statistically significant body weight increase of 49.5% compared to baseline. In the groups treated with DO-190 at 35 mg/kg and ethambutol at 50 mg/kg, the weight gain was 29% and 30%, respectively. Despite the marked weight gain at the higher dose of DO-190 (70 mg/kg), repetitive stereotypic movements (circling on the cage grid) were observed, which may indicate potential neurological effects. Exposure to DO-209 resulted in a smaller weight gain

(approximately 13–16%), which may reflect a different toxicological profile and potentially better tolerability.

The results of the blood count analysis in the experimental mouse model are presented in Table 13. Administration of INH led to a statistically significant decrease in red blood cell count, hemoglobin, and hematocrit—by 28%, 21%, and 20%, respectively—compared to the control group and reference values for mice. The white blood cell (WBC) count increased by 70% compared to controls, but the values remained within the physiological range. No changes in platelet levels were observed after 14 days of oral INH administration. In animals treated with both doses of compound 3a, no statistically significant deviations from the reference values were found, indicating that the tested compounds did not exert adverse effects on hematopoiesis.

Table 13. Hematological parameters after 14-day administration of INH and the aroylhydrazones 3a and 3d.

Hematological parameters	Controls	INH	3a	3a	3d	3d	Reference values
		50 mg/kg	125 mg/kg	250 mg/kg	125 mg/kg	250 mg/kg	
WBC x 10^9/L	5,8 ± 0,34	9.9±0.54*	6.3±0.36^{+}	7.4±0.44^{*+}	8.2±0.28^{*+}	7.7±0.33^{*+}	**2.9 – 15.3**
RBC x 10^{12}/L	7.39 ± 0.6	5.35±0.2*	6.84±0.3^{+}	6,97± 0,3^{+}	7.21±0.16^{+}	7.62±0.24^{+}	**5.6 – 7.89**
Hgb g/L	142 ± 7.6	112 ±2.2*	127 ±5.4^{+}	129 ± 3.8^{+}	132.2±4.2^{+}	130.2±3.7^{+}	**120 - 150**
HCT %	41.3 ± 1.8	33.3±2.1*	37.2±2.6^{+}	38.2 ±1.8^{+}	39.6 ± 0.8^{+}	40,1 ± 1,2^{+}	**36 - 46**
PLT 10^9/L	886 ± 126	789 ±183	979 ±238	638 ± 181	729 ± 203	864 ± 212	**100 - 1610**

$p < 0.05$ compared to controls; + $p < 0.05$ compared to EMB. Results are expressed as mean ± SD (n = 6). Statistical significance was assessed using the nonparametric Mann-Whitney U test. Values of $p \leq 0.05$ were considered statistically significant. Abbreviations: WBC – white blood cells; RBC – red blood cells; PLT – platelets; Hb – hemoglobin; and Ht – hematocrit.

The results of the serum biochemical analysis in the experimental mouse model, presented in Table 14, reveal a statistically significant increase in parameters related to liver and kidney function after 14 days of oral administration of INH. This increase includes indicators such as liver enzyme activities and levels of urea and creatinine, suggesting a potential impact on these organs. In contrast, animals treated with aroylhydrazones 3a and 3d at doses of 125 and 250 mg/kg did not exhibit the same effects. The analysis of biochemical parameters shows statistically significant changes following 14-day oral administration of INH. The transaminases ASAT and ALAT increased by 52% and 67%, respectively, compared to the control group and reference values for mice.

Moreover, albumin and total protein levels significantly decreased by 23% and 26%, respectively, which may indicate suppressed synthetic activity of the liver. Urea and creatinine increased by 49% and 29%, respectively, suggesting possible impairments in kidney function.

Despite these changes, no significant alterations in blood glucose levels were observed in any of the experimental groups.

Table 14. Biochemical parameters in serum after 14-day administration of INH and aroylhydrazones 3a and 3d at doses of 125 and 250 mg/kg.

Biochemical parameters	Controls	INH	3a	3a	3d	3d	Reference values
		50 mg/ kg	125mg/kg	250 mg/kg	125 mg/kg	250 mg/kg	
GLU mmol/L	6.4 ± 0.47	6.3 ± 0.36	7.1 ± 0.24	6.8 ± 0.22	7.0 ± 0.16	4.2 ± 7.5	**6.4 ± 0.47**
UREA mmol/L	9.1 ± 0,12	13.6 ±0.36*	8.8 ±0.28+	11.5 ±0.22+	8.7 ±0.26+	8.4 ±0.23+	**3.27 – 12.1**
CREATμmol/ L	98.3 ± 2,3	126.6±8.2*	95,6 ± 6.6+	86.4 ± 5.6+	88.2 ± 3.1+	92.2 ± 4.4+	**35 – 120**
UA μmol/L	195 ± 18,9	196 ± 20.7	163 ± 23.4	194 ± 17.7	199 ± 14.6	201.3 ± 12	**0 - 300**
TP g/L	58.1 ± 2.2	43.2 ± 3.1*	54.3 ± 2.6+	58.6 ± 3,6+	56.6 ± 4.2+	52.2 ± 5.1+	**53 – 63**
ALB g/L	27.9 ± 1.8	21.6 ± 1.7*	26,6 ± 2.2+	27.3 ± 3.1+	28.5 ± 3.3+	28.2 ± 2.8	**26 - 29**
ASAT U/L	83 ± 4.1	86 ± 5.4	121.2±3.2ab	122.2 ±2.1ab	91 ± 3.8	98 ± 4.8	**65 - 122**
ALAT U/L	58 ± 4.2	59 ± 6.1	80.2 ±2.2ab	79.3 ± 1.3db	62.2 ± 4.3	88.4 ±3.6abc	**55 - 80**
T-Bil μmol/L	5.6 ± 0.48	6.0 ± 0.28	8.2 ±0.41ab	8.4 ± 0.8ab	4.4 ± 0.42	6.3 ± 0.38	**3.9 - 9.6**
D-Bil μmol/L	3.4 ± 0.86	3.5 ± 0.84	3.8 ±0.31	4.1 ± 0.61	3.4 ±0.56	4.9± 0.24	**0 - 6.8**

*$p < 0.05$ compared to controls; +$p < 0.05$ compared to INH. Results are expressed as mean ± SD (n = 6). Statistical significance was assessed using the nonparametric Mann-Whitney U test. Values of $p \leq 0.05$ were considered statistically significant. Abbreviations: Glu, glucose level; CREAT, creatinine; UA, uric acid; TP, total protein; Alb, albumin; AST, aspartate aminotransferase; ALT, alanine aminotransferase; T-Bil, total bilirubin; and D-Bil, direct bilirubin.

No statistically significant deviations in hematological and biochemical parameters were found in animals treated with compounds 3a and 3d, indicating good tolerability of these substances. The weight gain and absence of significant changes in hematological, biochemical, and pathomorphological parameters in blood, liver, small intestine, and kidneys suggest that compounds 3a and 3d are well tolerated when administered at appropriate doses.

The results of the complete blood count and biochemical parameters analysis in mice after 14 days of repeated administration of nitrofuranylamides DO-190 and DO-209 show a slight increase in WBC count (Table 15). This increase is particularly pronounced at higher doses compared to the control group. However, these changes remain within the reference values for the species and do not suggest the presence of pathological alterations. No significant changes were observed in other hematological parameters compared to the control group.

Table 15. Hematological parameters after 14-day administration of EMB and nitrofuranylamides DO190 and DO209.

Hematological parameters	Controls	EMB	DO190	DO190	DO209	DO209	Reference values
		50 mg/ kg	35mg/kg	70mg/ kg	125mg/ kg	250 mg/kg	
WBC x 10^9/L	5.8 ± 0.34	6.4± 0,5[a]	7.8± 0,6[a]	7.1± 0.7	8.23±0.13[b]	6.8± 0.6	**2.9 – 15.3**
RBC x 10^{12}/L	7,39 ± 0,6	7.06 ±0.4	6.36± 0,8	7.03± 0.5	6.02± 0.2 [b]	7.23± 0.7	**5,6 - 7,89**
Hgb g/L	142 ± 7,6	142 ±7.2	142± 2.6	136± 3.2	128± 4.1	135± 2.4	**120 - 150**
HCT %	41,3 ± 1,8	44 ±2.4	41± 3.2	42.4± 2.2	43.2± 3.1	42.2± 3.7	**36 - 46**
PLT 10^9/L	886 ± 126	789 ±96	881± 123	865± 105	932± 116	888± 121	**100 - 1610**

a $p < 0.05$ compared to controls; b $p < 0.05$ compared to EMB. Results are expressed as mean ± SD (n = 6). Statistical significance was assessed using the nonparametric Mann-Whitney U test. Values of $p \leq 0.05$ were considered statistically significant. Abbreviations: WBC – white blood cells; RBC – red blood cells; PLT – platelets; Hb – hemoglobin; and Ht – hematocrit.

Table 16. Biochemical parameters in serum from experimental animals after 14 days of administration of EMB and nitrofuranylamides DO190 and DO209.

Biochemical parameters	Controls	EMB	DO 190	DO 190	DO 209	DO 209	Reference values
		50 mg/ kg	35mg/kg	70 mg/kg	125 mg/kg	250 mg/kg	
GLU mmol/L	6.2 ± 0.12	7.1± 0.4	6.3 ± 0.5	7.3± 0.32	6.5± 0.41	8.8±0.29[ab]	**4.2 – 7.5**
UREA mmol/L	7.1 ± 0.32	8.0± 0.36	11.4±0.31[ab]	12.6±0.28[ab]	6.8±0.22	13.±.22[ab]	**3.27 – 12.1**
CREAT µmol/L	88 ± 12.3	82± 12.8	92.3± 8.2	102.2± 11.6	85± 16.2	79± 12.6	**35 – 120**
UA µmol/L	236 ± 11.4	385±20.3d	286.3±9.1[ab]	298±11.3[db]	243±133	261± 12.3	**0 - 300**
TP g/L	58 ± 3.2	53± 4.6	55.2 ± 2.8	58.1± 3.1	54± 5.3	56± 3.3	**53 – 63**
ALB g/L	27 ± 1.3	28± 1.2	27.2± 0.8	26.8± 1.6	26± 2.2	27± 3.1	**26 - 29**
ASAT U/L	83 ± 4.1	86± 5.4	121.2±3.2[ab]	122.2±2.1[ab]	91± 3.8	98± 4.8	**65 - 122**
ALAT U/L	58 ± 4.2	59± 6.1	80.2± 2.2[ab]	79.3±1.3d	62.2±4.3	88±43.6[abc]	**55 - 80**
T-Bil µmol/L	5.6 ± 0.48	6.0± 0.28	8.2± 0.41[ab]	8.4± 0.8[ab]	4.4±0.42	6.3± 0.38	**3.9 - 9.6**
D-Bil µmol/L	3.4 ± 0.86	3.5± 0.84	3.8± 0.31	4.1± 0.61	3.4±0.56	4.9± 0.24	**0 - 6.8**

a $p < 0.05$ compared to controls; b $p < 0.05$ compared to EMB; c $p < 0.05$ compared to reference values. Results are expressed as mean ± SD (n = 6). Values of $p \leq 0.05$ were considered statistically significant. Abbreviations: Glu, glucose level; CREAT, creatinine; UA, uric acid; TP, total protein; Alb, albumin; AST, aspartate aminotransferase; ALT, alanine aminotransferase; T-Bil, total bilirubin; and D-Bil, direct bilirubin.

6. Pathomorphological assessment of changes in target organs after administration of aroylhydrazones (3a and 3d) and nitrofuranylamides (DO 190 and DO 209) compared to control groups

6.1. Pathomorphological assessment of liver changes

Histological analysis (Figure 15) showed that compounds 3a and 3d did not cause significant pathological changes in the liver after 14 days of administration. At doses up to 250 mg/kg, the lobular structure was preserved with minimal ballooning degeneration and limited cholestasis. Higher doses (3000 mg/kg) led to mild collagenization without fibrosis. Mild steatosis was also observed, confirming the favorable hepatotoxicological profile of the compounds.

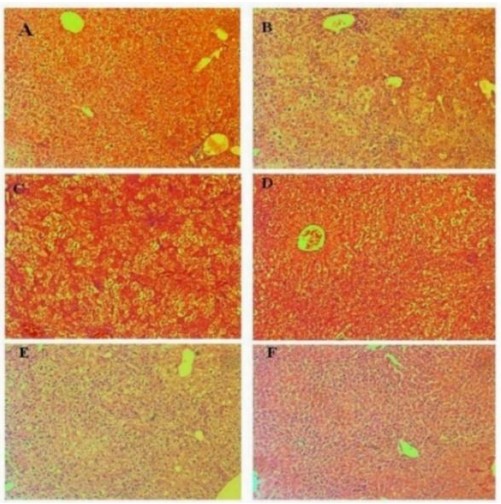

Figure 15. Pathomorphological findings in the liver of mice after oral administration of INH and aroylhydrazones 3a and 3d.

Legend: (A) Control group – untreated; (B) INH, 50 mg/kg; (C) 3a (VAL-SNN), 125 mg/kg; (D) 3a (VAL-SNN), 250 mg/kg; (E) 3d, 125 mg/kg; (F) 3d, 250 mg/kg; Magnification 100×.

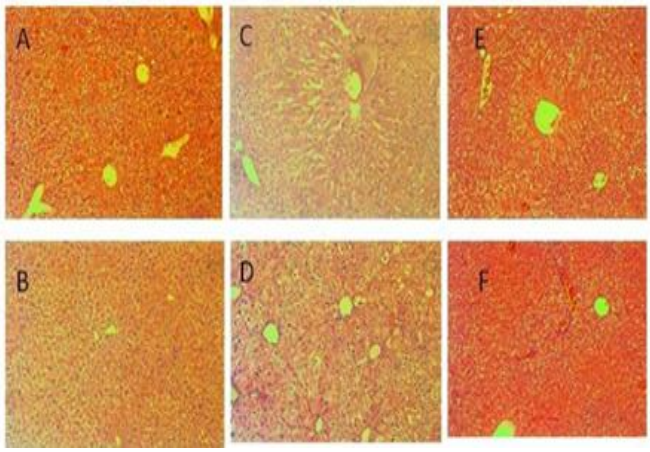

Figure 16. Pathomorphological findings in the liver of mice after oral administration of INH, EMB, and nitrofuranylamides DO 190 and DO 209.

Legend: (A) Control group – untreated; (B) EMB, 50 mg/kg; (C) DO 190, 35 mg/kg; (D) DO 190, 70 mg/kg; (E) DO 190, 800 mg/kg; (F) DO 209, 3000 mg/kg; Magnification 100×

Pathomorphological analysis of the liver in mice treated with nitrofuranylamides DO-190 and DO-209 revealed no significant pathological changes (Figure 16).

Histological analysis of the liver showed preserved lobular architecture with minimal changes — mild intrahepatic cholestasis, passive venous hyperemia, and slight sinusoidal dilation. No fibrosis, inflammation, or hepatocyte loss were observed. Ballooning degeneration affected 8–18% of the cells, and steatosis was up to 3%. At 3000 mg/kg DO-209, moderate degenerative changes were detected without severe toxicity, with limited cellular damage confirmed by the sporadic presence of autophagic vacuoles.

1.2.1. Pathomorphological assessment of changes in the kidneys

Examinations of kidney tissue after 14-day administration of aroylhydrazone compounds (3a and 3d) showed no significant deviations from normal renal structure (Figure 17).

In the control group, the kidney structure was fully preserved without pathological changes. In the group treated with INH (50 mg/kg), the distal tubules also maintained their structure, with minimal epithelial alterations.

In the groups treated with derivative 3a (125 and 250 mg/kg), only minimal circulatory lesions and interstitial edema were observed, without tubulitis, atrophy, or glomerulitis. Similarly, groups treated with 3d showed insignificant variations in kidney structure without toxic effects. Histological analysis did not reveal significant pathological changes in the proximal and distal tubules, vessels, or mesangium. Possible vascular hyperemia did not lead to structural damage and did not affect renal function.

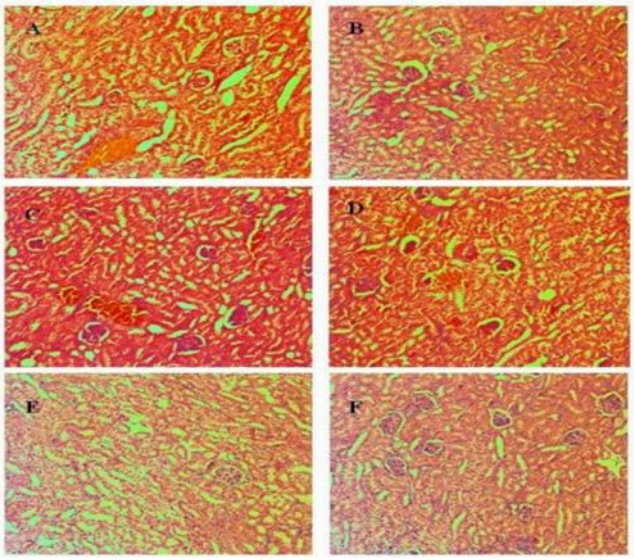

Figure 17. Pathomorphological findings in the kidneys of mice after oral administration of INH and aroylhydrazones 3a and 3d.

Legend: (A) Control group – untreated; (B) INH, 50 mg/kg; (C) 3a, 125 mg/kg; (D) 3a, 250 mg/kg; (E) 3d, 125 mg/kg; (F) 3d, 250 mg/kg; Magnification 100×.

At high doses, mild adaptive changes were observed in the medium-sized region and periglomerular interstitium, which did not lead to permanent damage. No pathological changes were found in the collecting ducts either. Examination of kidney tissue after treatment with DO-190 and DO-209 revealed no significant topographical alterations and confirmed preserved renal structure and function (Figure 18).

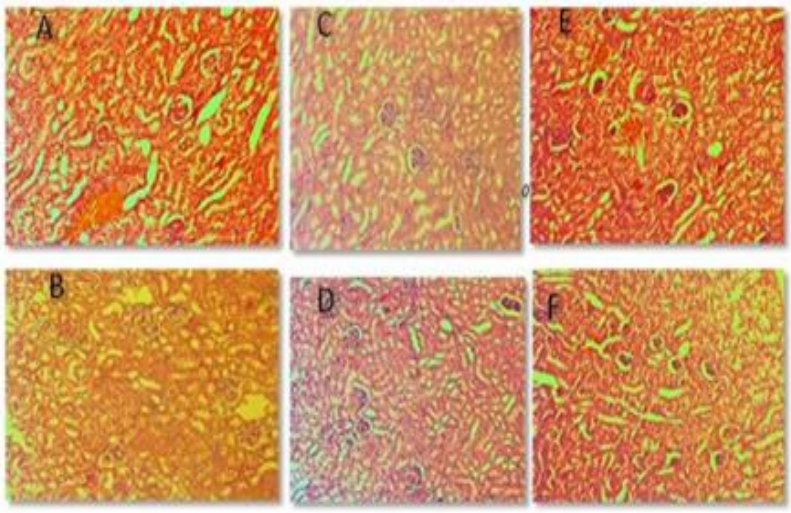

Figure 18. Pathomorphological findings in the kidneys of mice after oral administration of INH, EMB, and nitrofuranylamides DO 190 and DO 209.

Legend: (A) Control group – untreated; (B) EMB, 50 mg/kg; (C) DO 190, 35 mg/kg; (D) DO 190, 70 mg/kg; (E) DO 190, 800 mg/kg; (F) DO 209, 3000 mg/kg; Magnification 100×.

The observed minimal alterations—such as interstitial edema, slight epithelial attenuation, and dilated luminal segments—are not associated with toxic damage. There are no signs of tubulitis, atrophy, or inflammatory processes. The data indicate that the tested compounds do not induce significant nephrotoxicity, even at high doses.

1.3. Pathomorphological Assessment of Changes in the Small Intestine

Following oral administration of the aroylhydrazone compounds (3a and 3d) and nitrofuranylamides (DO-190 and DO-209), histological analysis of the small intestine in mice reveals dose-dependent variations in cellular activity and mucosal structure (Figures 19 and 20). Inflammatory processes are mild, with leukocyte density below 10% in the lamina propria, without significant variation among the animals.

Pathomorphological analysis of the small intestinal tissue across all experimental groups shows no significant damage or inflammatory reactions. Animals treated with INH, 3a, 3d, EMB, DO-190, and DO-209 exhibit only minimal changes in the crypt-villus architecture without inflammatory infiltration or significant atrophy. Leukocyte infiltration is limited, and the epithelium remains intact, indicating the absence of toxic effects on the intestinal mucosa, even at higher doses.

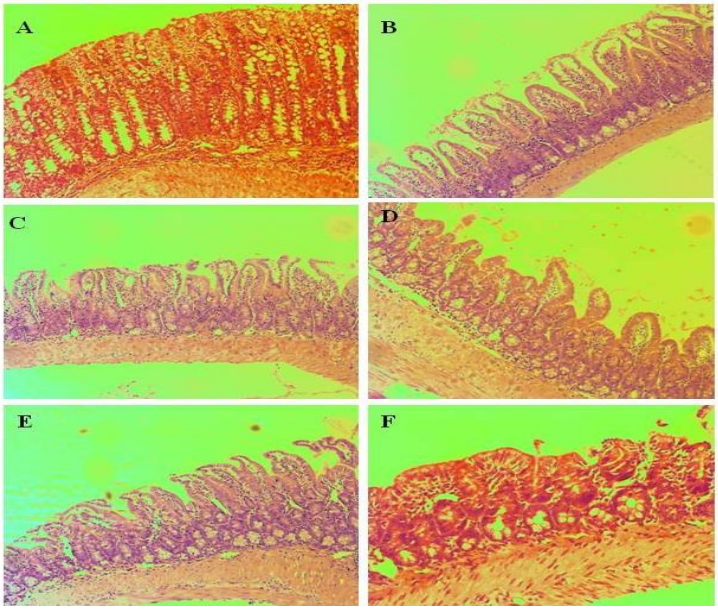

Figure 19. Pathomorphological findings in the small intestines of mice after oral administration of INH and aroylhydrazones 3a and 3d. Legend:A. Control group – untreated; B. INH, 50 mg/kg; C. 3a, 125 mg/kg; D. 3a, 250 mg/kg; E. 3d, 125 mg/kg; F. 3d, 250 mg/kg Magnification 100×

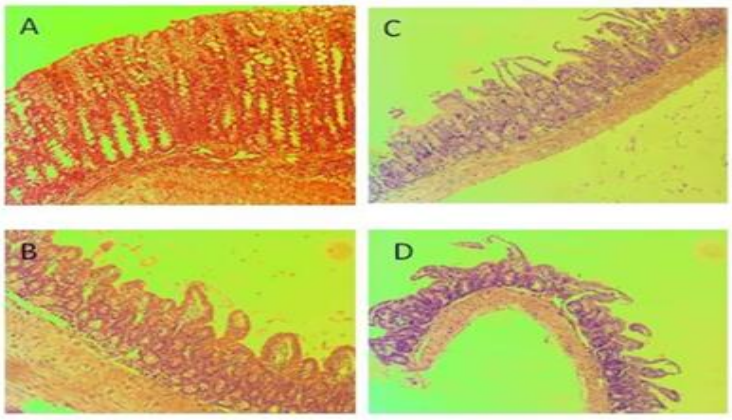

Figure 20. Pathomorphological findings in the small intestines of mice after oral administration of INH, EMB and nitrofuranylamides DO 190 and DO 209. Legend: (A) Control group – untreated, (B) EMB, 50 mg/kg, (C) DO 190, 35 mg/kg, (D) DO 190, 70 mg/kg, Magnification 100×.

Histological analysis of the small intestinal tissue in mice treated with EMB, DO-190, and DO-209 shows minimal structural changes without significant inflammatory reactions. In the control group, the epithelium is intact, with no erosion, infiltration, or defects affecting the lamina muscularis mucosae.

The results of this assessment highlight the need for careful dose optimization. The histopathological changes observed with DO-190 and DO-209 indicate dose-dependent toxicity, with higher doses causing more pronounced hepatic alterations. In contrast, the aroylhydrazones (3a and 3d) demonstrate a favorable safety profile, causing minimal or no significant organ damage. These findings support the hypothesis that lower doses of

nitrofuranylamides may be safer, reducing the risk of hepatotoxicity while maintaining therapeutic efficacy. This suggests that future studies should focus on determining the optimal therapeutic window that balances efficacy and safety.

This study examined the hepatotoxicity induced by INH, aroylhydrazone compounds, and nitrofuranylamides under experimental conditions. Data from histological examinations show that despite minimal pathological changes observed after exposure to INH and aroylhydrazones, there are no serious hepatotoxic effects leading to pronounced necrosis or fibrosis in the mouse liver, as also reported in the studies of Tostmann (2008).

It is known that hydrazine, the main toxic metabolite of isoniazid, induces steatosis, hepatocyte vacuolation, and glutathione depletion, resulting in lipid vacuole formation and mitochondrial swelling in periportal and midzonal hepatocytes (Tostmann et al., 2007). Despite this theoretical data, our results do not show significant morphological alterations fully corresponding to the described toxicity symptoms, although minimal signs of ballooning degeneration were observed in some experimental groups.

Regarding rifampicin (RIF), although not included in this study, data showing it can cause transient hyperbilirubinemia and liver lesions characterized by hepatocellular changes and centrilobular necrosis associated with cholestasis (Combrink et al., 2020). Human studies indicate that rifampicin can lead to serious liver changes such as lymphocytic infiltration, focal cholestasis, and increased fibrosis, sometimes resulting in micronodular cirrhosis. While these effects were not observed in our models, the potential for drug-induced toxic changes with agents like rifampicin remains significant and requires careful monitoring and risk assessment during their use, especially in combination with other medications.

7. Assessment of Oxidative Stress Markers

7.1 Assessment of Oxidative Stress Markers after Treatment with Aroylhydrazones 3a and 3d

Table 16. *In vitro* redox-modulating properties of 3a and 3d

Parameter	Fe^{2+}	DPPH	ABTS
Compounds	**IC_{50} [mg/ml]**	**IC_{50} [mg/ml]**	**IC_{50} [mg/ml]**
3a	85.14 *	18.69 *	40.35 *
3d	76.29 *	47.5 *	89.47 *
Trolox	18.2	8.92	24.8

*P<0,01 Compared to the control

The results from the assessment of the redox-modulating capacity of the active

compounds are presented in Table 16.

Using the DPPH assay, we evaluated the radical scavenging activity of the substances.The analysis is based on the ability to transfer a hydrogen atom (Li, D.L. et al., 2009), and the activity is associated with the presence of a polar-bound hydrogen in the molecule of the tested substrate.

Compounds 3a and 3d demonstrated significant radical scavenging activity in both the DPPH and ABTS assays, with recorded IC50 values (mg/ml) suggesting the presence of antioxidant activity in the model systems, which is likely related to the observed biological tolerance and absence of toxicity *in vivo.*

However, it should be noted that both DPPH and ABTS radicals do not occur naturally, which raises questions about their direct role in biological processes.

The effect of INH on lipid peroxidation levels, measured by the amount of TBARS as a marker of oxidative stress in liver homogenate supernatant, is shown in Figure 21.

Following the administration of INH (50 mg/kg), the MDA level increased by over 35%, while compound 3a at both doses slightly decreased MDA compared to the control. Compound 3d did not significantly alter MDA levels. *In vivo,* 3a showed a better effect against iron-induced lipid peroxidation compared to *in vitro* models. The MDA content reflects the degree of lipid peroxidation and the level of damage caused by pro-oxidants (Niedernhofer, L.J. et al., 2007).

Alongside the reduction of MDA, we found that INH decreased total GSH levels by approximately 40% (Figure 22). Compounds 3a at both doses showed GSH levels comparable to those of INH, while 3d at both doses showed levels close to those of the control animals.

GSH is a key antioxidant that regulates redox processes and inflammation in the body. Disruptions in its homeostasis are often associated with liver dysfunctions (Chen et al., 2013). GSH neutralizes reactive oxygen species and supports the activity of glutathione peroxidase, as well as the regeneration of vitamins C and E. GSH deficiency increases the risk of cellular damage in patients with tuberculosis, HIV, and diabetes (Nair et al., 2021).

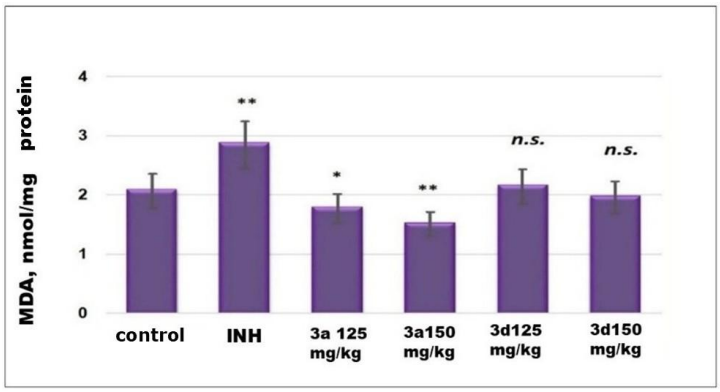

Figure 21. Endogenous MDA content in liver homogenate of the experimental groups. *P < 0.05 compared to controls; **P < 0.01 compared to controls; n.s. – not significant compared to INH. Results are expressed as mean ± SD (n = 6). Statistical significance was assessed using the nonparametric Mann–Whitney U test. Values of $p \leq 0.05$ were considered statistically significant.

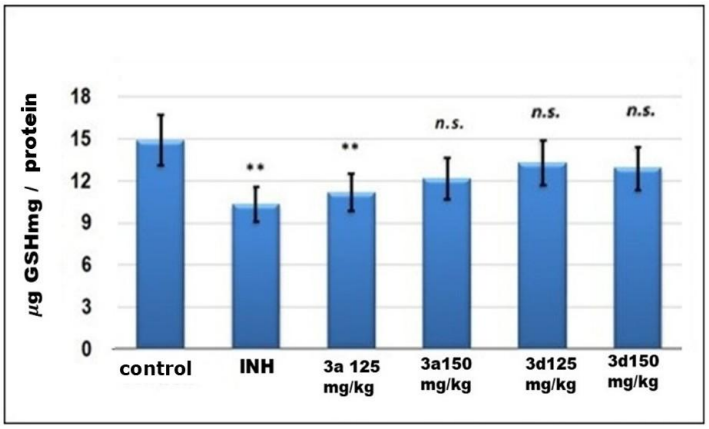

Figure 22. Endogenous GSH content in liver homogenate of the experimental groups. *p < 0.05 compared to controls; **p < 0.01 compared to controls; n.s. – not significant compared to controls. Results are expressed as mean ± SD (n = 6). Statistical significance was assessed using the nonparametric Mann-Whitney U test. Values of $p \leq 0.05$ were considered statistically significant.

The results from Figure 23 show that INH increases GPx activity by approximately 35% and SOD activity by 25% compared to the control samples. In contrast, compounds 3a and 3d do not cause statistically significant changes in the activities of these enzymes, with compound 3d restoring GPx levels to values close to the controls. Furthermore, INH causes about a 30% reduction in glutathione levels, whereas the newly synthesized analogues maintain glutathione levels.

The data obtained suggest that compounds 3a and 3d demonstrate a stable redox-modulating potential by inducing compensatory changes in enzyme activities and stabilizing the levels of oxidative stress markers. This identifies them as potential therapeutic agents for limiting oxidative damage, especially in the context of tuberculosis infection and its associated liver toxicity.

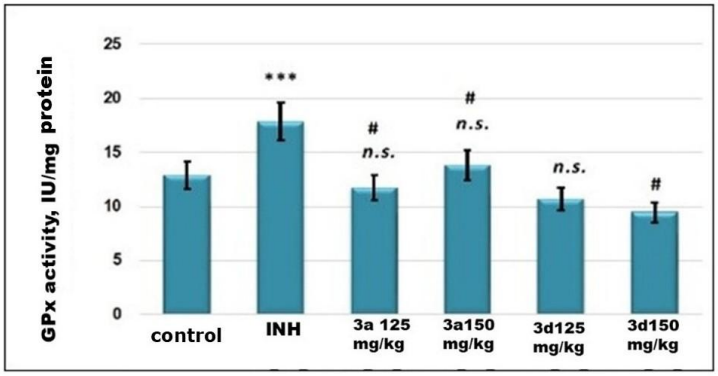

Figure 23. Glutathione peroxidase activity in the liver supernatant of the experimental groups.*P < 0.001 vs. controls; #P < 0.01 vs. INH 50 mg/kg; n.s. – not significant vs. controls.

Results are expressed as mean ± SD (n = 6). Statistical significance was assessed using the nonparametric Mann-Whitney U test. Values of $p \leq 0.05$ were considered statistically significant.

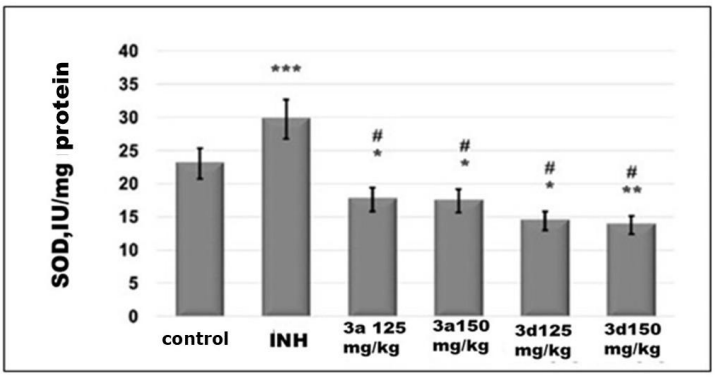

Figure 24. Superoxide dismutase (SOD) activity in the liver supernatant of the experimental groups. ***P < 0.001 vs. controls; **P < 0.01 vs. controls; P < 0.05 vs. controls; #P < 0.001 vs. INH 50 mg/kg.*Results are expressed as mean ± SD (n = 6). Statistical significance was assessed using the nonparametric Mann-Whitney U test.

The enzymes GPx and SOD act synergistically by eliminating superoxide and hydroxyl radicals, as well as hydrogen peroxide, thereby maintaining glutathione balance within the cells. In our study, we found that compounds 3a and 3d did not induce significant changes in the activity of these enzymes compared to untreated control animals, whereas INH increased their activity. The results from the *in vivo* experiments indicate that compounds 3a and 3d have the potential to restore oxidative stress markers and exhibit a similar redox-modulating effect across different doses. Therefore, they can be considered as potential drug candidates for controlling oxidative damage associated with hepatotoxicity, especially in the context of tuberculosis infection.

7.2 Evaluation of oxidative stress markers after treatment with nitrofuranilamides (DO 190 and DO 209).

The results presented in Figure 25 illustrate changes in MDA content in liver tissue following exposure to the nitrofuranilamides DO 190 and DO 209. Elevated MDA levels

indicate increased lipid peroxidation, which is associated with oxidative stress and damage to cellular membranes.

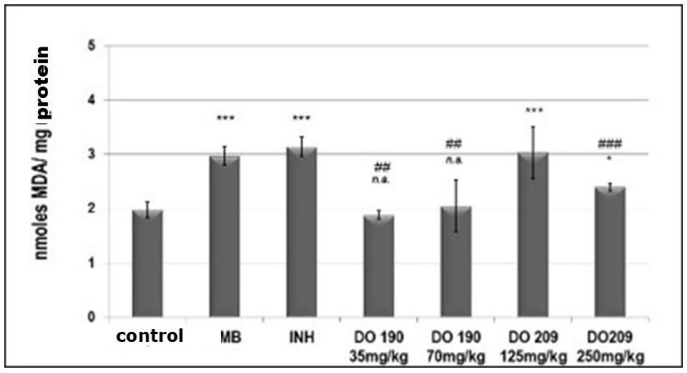

Figure 25. Endogenous MDA content in the liver homogenate of the experimental groups. p < 0.05 compared to controls; *** p < 0.001 compared to controls; ns — not significant compared to controls; ## p < 0.01 compared to EMB and INH; ### p < 0.001 compared to EMB and INH. Results are expressed as mean ± SD (n = 6). Statistical significance was assessed using the non-parametric Mann-Whitney U test. Values of $p \leq 0.05$ were considered statistically significant.

In the groups treated with both INH and EMB, the level of MDA increased by more than 35%. Doses of 35 and 70 mg/kg of compound DO-190 did not cause significant deviations compared to control animals ($p < 0.001$). The endogenous MDA content for compound DO-209 at a dose of 125 mg/kg showed comparable values to the INH and EMB controls, but at a dose of 250 mg/kg, the value was reduced.

The results in Figure 26 show that in the groups treated with DO-190 at both doses, significant dose-dependent decreases in intracellular total glutathione levels were observed.

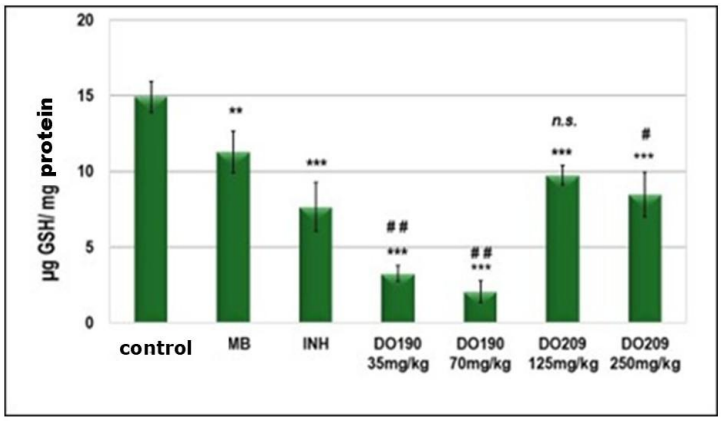

Figure 26. Endogenous GSH content in the liver homogenate of the experimental groups. ***p < 0.01 compared to controls; ns - not significant compared to controls; p < 0.01 compared to controls; #p < 0.01 compared to EMB; ##p < 0.01 compared to EMB and INH. Results are expressed as mean ± SD (n = 6). Statistical significance was assessed using the non-parametric Mann-Whitney U test. Values of $p \leq 0.05$ were considered statistically significant.

The total glutathione levels in the groups treated with DO-190 were nearly 5 times lower compared to the untreated controls ($p < 0.001$), almost 3 times lower compared to the EMB-treated group ($p < 0.01$), and more than 2 times lower compared to the INH-treated group ($p < 0.01$). In contrast, DO-209 at both doses depleted liver glutathione by more than 25% compared to the untreated control animals.

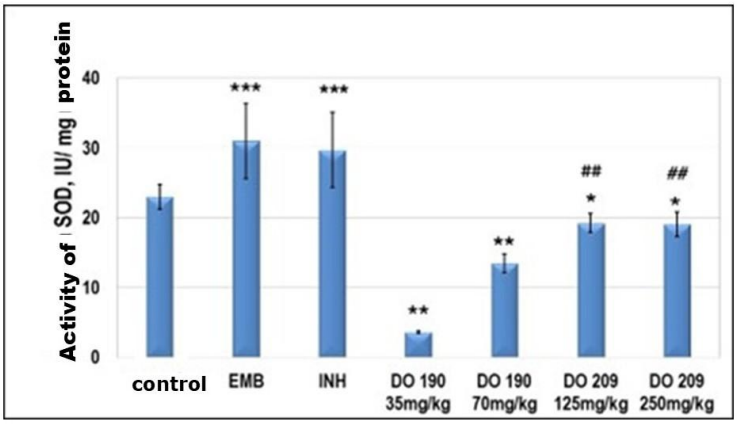

Figure 27. SOD activity in the liver supernatant of the experimental groups. *** $p < 0.001$ compared to controls; ** $p < 0.01$ compared to controls; * $p < 0.05$ compared to controls; ## $p < 0.01$ compared to EMB and INH. Results are expressed as mean ± SD (n = 6). Statistical significance was assessed using the non-parametric Mann-Whitney U test. Values of $p \leq 0.05$ were considered statistically significant.

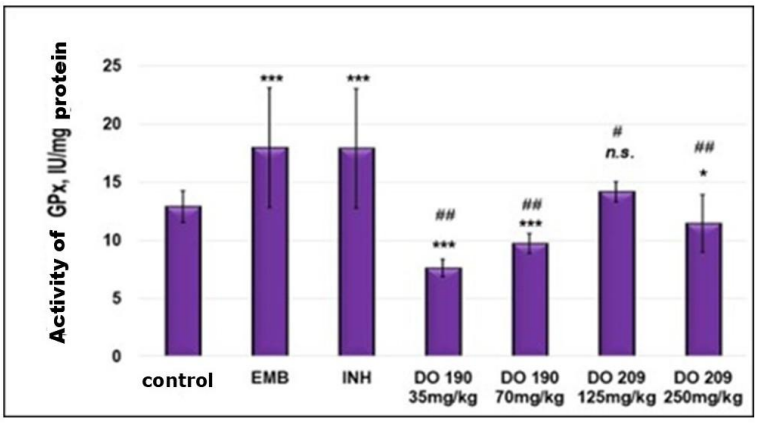

Figure 28. Glutathione peroxidase activity in the liver supernatant of the experimental groups. ***$p < 0.001$ compared to controls; *$p < 0.05$ compared to controls; #$p < 0.05$ compared to INH 50 mg/kg; ##$p < 0.01$ compared to INH 50 mg/kg; ###$p < 0.001$ compared to INH 50 mg/kg; ns — not significant compared to controls. Results are expressed as mean ± SD (n = 6). Statistical significance was assessed using the non-parametric Mann-Whitney U test. Values of $p \leq 0.05$ were considered statistically significant.

In animals treated with INH and EMB, an increased SOD activity was observed, indicating effective protection against oxidative stress. At the same time, animals treated with DO-190 showed a significant decrease in SOD activity at both doses ($p < 0.001$), while DO-209 exhibited much lower activity compared to controls (Figure 27). This suggests that DO-

190 and DO-209 may impair the normal antioxidant defense of the cells, which could lead to a higher risk of oxidative damage.

The GPx activities in the experimental groups are presented in Figure 28. INH and EMB increased GPx activity compared to controls, whereas DO-190 significantly decreased it at both doses ($p < 0.001$). A similar effect was observed with the higher dose of DO-209 (250 mg/kg). In mice treated with 250 mg/kg, GPx activity showed a slight decrease compared to controls ($p < 0.05$) and was significantly lower than in groups treated with EMB and INH ($p < 0.01$). These effects suggest a relatively safe toxicological profile for the newly synthesized compounds under investigation.

The results of the present study show that the compound DO-190, administered at both tested doses, leads to a decrease in intracellular glutathione levels, which is accompanied by a compensatory increase in the activity of the antioxidant enzymes SOD and GPx. These adaptive changes likely limited the damage to cell membranes caused by lipid peroxidation and prevented the accumulation of high levels of MDA.

8. *In vitro* mutagenesis and isolation of resistant mutants of *M. tuberculosis* H37Rv with subsequent whole genome sequencing

After selection of active compounds through preliminary tests, an *in vitro* mutagenesis assay was performed using *M. tuberculosis* H37Rv. Subsequently, resistant mutants were selected, DNA was isolated from the resulting clones. A classical experimental approach was used, where each clone was recultivated on media containing 2×, 4×, and 8× MIC of the respective compound. Afterwards, DNA extraction and whole genome sequencing were performed separately for each clone (Figure 29).

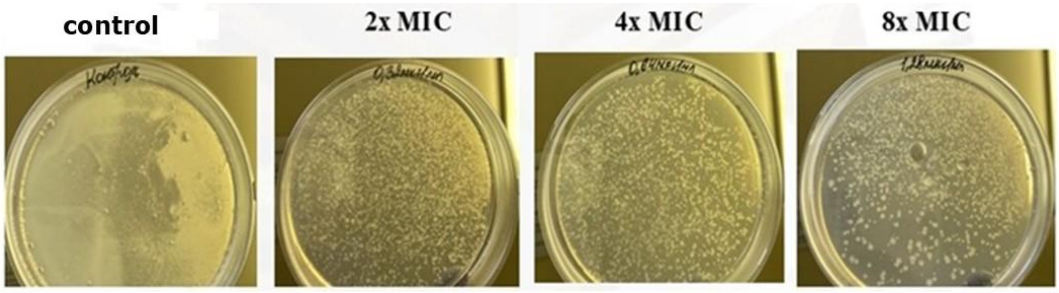

Figure 29. *In vitro* mutagenesis of *M. tuberculosis* H37Rv strain with compounds at concentrations of 2×, 4×, and 8× MIC.

The whole genome sequencing data was subjected to comparative SNP analysis to identify mutations associated with resistance to the aroylhydrazone MLT_FUR (Table 17). Analysis of a *M. tuberculosis* clone grown at increased concentrations of the compound revealed mutations in the genes Rv2702, Rv0506, and Rv3755c. This reflects the adaptive

response of the bacteria to drug pressure. The identified genes are involved in key cellular processes such as metabolism, redox balance, and regulation of gene expression (Table 18).

Table 17. List of DNA mutations identified in isolated *M. tuberculosis* H37Rv mutants after cultivation with the newly synthesized compounds

Compound and Concentration	Position and Mutation	Gene	Position and Mutation	Codon, Nucleotide, and Amino Acid Change	PAM1	SIFT	Mutant Reads, %	Mutation Type
MLT_FUR 0.28 µg/ml (4× MIC)	4201587 T>C	Rv3755c	302 A>G	101 CAC→CGC, H→R	10	>0.05	94	Non-synonymous
MLT_FUR 0.28 µg/ml (4× MIC)	3017408 del_C	Rv2702 / ppgK	551 del_C	184 frameshifts	-	-	94	Frameshift
MLT_FUR 0.56 µg/ml (8× MIC)	597110 A>G	Rv0506 / mmpS2	352 A>G	118 AGC→GGC, S→G	21	>0.05	100	

The mutation in the Rv2702 gene (ppgK) affects metabolic pathways related to lipid synthesis and drug tolerance in *M. tuberculosis*. It causes a frameshift at codon 184, which likely results in gene inactivation by truncating the protein by approximately 30%. ppgK is an essential gene required for bacterial growth *in vivo* and is associated with induced drug tolerance, especially under nutrient deprivation conditions, where PDIM lipid production is critical (Marrero et al., 2013; Block et al., 2023).

Rv0506 (mmpS2) is involved in efflux systems and is linked to the active transport of drugs out of the cell—a well-known mechanism of resistance.

In the MLT_FUR-resistant clone, a nonsynonymous SNP mutation was identified in Rv3755c (101H>R). Although the functional role of this gene is unknown, in silico analyses suggest that the mutation is tolerated (PAM1 = 10; SIFT – tolerant).

Table 18. Identified mutations found in isolated *M. tuberculosis* H37Rv mutants after cultivation with the newly synthesized compounds.

Gene	Protein Name	Protein Function	Gene Category
Rv2702 / Ppgk	Polyphosphate glucokinase Ppgk	Catalyzes phosphorylation of glucose using polyphosphate or ATP as donors	Intermediate metabolism and respiration
Rv0506 / mmpS2	Membrane protein MmpS2	Unknown	Cell wall and cell processes
Rv3755c	Rv3755c	Hypothetical protein	Conserved hypothetical genes

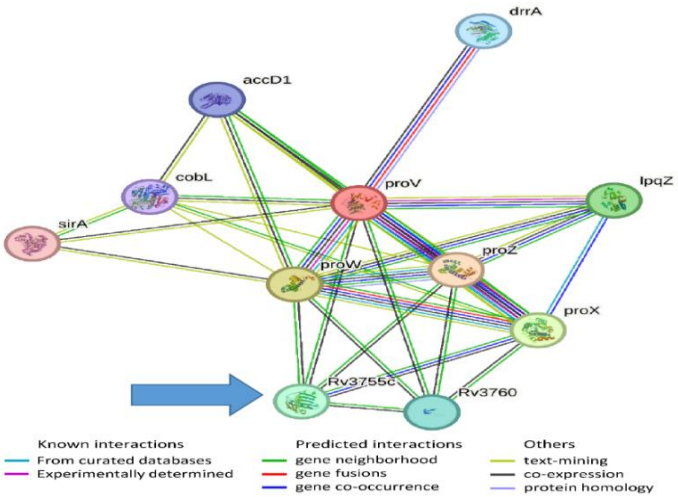

Figure 30. Gene-gene interaction network including the gene *Rv3755c*; p-value: 1.52e-07. The arrow indicates the *Rv3755c* gene.

The gene network surrounding Rv3755c includes genes encoding ABC transport systems (Figure 30), which suggests a role in transport and possibly in drug resistance. ABC transporters participate in the transfer of various molecules, including antibiotics, out of the cell (Cassio Barreto de Oliveira et al., 2020).

The mutation in Rv3755c (identified in 94% of the reads) may contribute to the adaptation of *M. tuberculosis* to MLT_FUR through increased efflux. According to Mycobrowser, the gene is non-essential *in vitro*, but is associated with delayed growth upon mutagenesis, suggesting a nonspecific tolerance mechanism (DeJesus MA et al., 2017; Minato Y et al., 2019; Sassetti CM et al., 2003).

Conclusion

In conclusion, the results of the study on the newly synthesized aroylhydrazone compounds 3a and 3d, as well as nitrofuranilamide derivatives DO190 and DO209, demonstrated activity against *M. tuberculosis* and *M. smegmatis*. They exhibit improved membrane permeability and stable binding to target enzymes, making them promising antitubercular candidates. Pathomorphological and biochemical analyses of target organs indicate that these compounds induce minimal changes and likely pose a low risk of drug-induced damage. Genomic sequencing revealed mutations associated with the rapid adaptation of mycobacteria to the selective pressure of the tested compounds. This suggests a nonspecific tolerance mechanism and highlights the importance of future studies aimed at clarifying the potential mechanisms of drug resistance and strategies to overcome it. The obtained results open new perspectives for further research focused on gathering additional evidence of their efficacy against tuberculosis.

Taken together, these findings highlight the significant advantage of the drug candidates investigated in clinical practice, especially in patients with impaired liver function or when long-term treatment is required.

V. Conclusions

1. The *in vitro* antimycobacterial activity against *M. smegmatis* and *M. tuberculosis* H37Rv of newly synthesized aroylhydrazones and nitrofuranilamides was demonstrated. Among them, two aroylhydrazones (3a and 3d) and two nitrofuranilamides (DO190 and DO209) were selected for their highest antimycobacterial activity.
2. It was established that the two aroylhydrazones (3a and 3d) and two nitrofuranilamides (DO190 and DO209) exhibit low cytotoxicity, with DO209 showing the strongest effect on tumor cells.
3. Energetic interactions between InhA and aroylhydrazones 3a and 3d, as well as nitrofuranilamides DO-190 and DO-209, were identified. The aroylhydrazones 3a and 3d showed lower binding energies than INH in both ligand-binding domains (2X22 and 4TZK), indicating more stable covalent binding to the enzymes. DO-190 and DO-209 exhibited lower binding energies than INH in all three ligand-binding domains (2X22, 4TZK, and 4FIY).
4. *In vivo* acute toxicity tests in mice showed that compounds 3a and 3d have good tolerability and no serious toxic effects. DO-190 and DO-209 differed significantly in toxicity, with DO-190 displaying a slightly increased toxic effect compared to DO-209.
5. Compounds 3a and 3d did not significantly affect the body weight of intraperitoneally treated mice during a 14-day subacute toxicity study and caused no noticeable toxic effects. DO-209 also showed better tolerability compared to DO-190.
6. Histological examination of mice treated with aroylhydrazones (3a and 3d) and nitrofuranilamides (DO-190 and DO-209) revealed minimal alterations in the cytoarchitecture of the liver, kidneys, and small intestine.
7. Changes in biochemical markers of oxidative stress in the liver showed that aroylhydrazones 3a and 3d suppress lipid peroxidation, restore intracellular low molecular weight antioxidant glutathione content, induce compensatory changes in antioxidant enzyme activities associated with hepatic toxicity, and exhibit better antiradical activity in model chemical systems compared to INH.

8. DO-190 induces dose-dependent reduction of malondialdehyde levels, depletion of intracellular glutathione, and changes in antioxidant enzyme activity.
9. DO-209 at higher doses improves liver redox homeostasis compared to the reference antibiotics INH and EMB.
10. Whole-genome sequencing revealed a mutation in gene Rv3755c, which belongs to a network including several ABC transporter genes. These ABC genes are involved in nutrient transport and uptake as well as drug efflux systems. This likely relates to the rapid adaptation of *M. tuberculosis* to the selective pressure of aroylhydrazone 3d and reflects a nonspecific tolerance mechanism.

VI. Contributions

1. For the first time in Bulgaria, a pharmacological screening of selected derivatives of EMB and INH was conducted. Lead compounds were identified — two aroylhydrazones and two nitrofuranilamide chemical compounds with the highest *in vitro* antimycobacterial activity.
2. The interactions of aroylhydrazone 3d with NAD+ and Tyr158 prove that 3d can be an inhibitor binding directly to InhA without requiring activation by KatG, making it effective against MDR-TB.
3. The two aroylhydrazone compounds (3a and 3d) and the two nitrofuranilamide compounds (DO190 and DO209) exhibit low cytotoxicity and good intracellular accumulation in normal and tumor cell lines, making them suitable drug candidates for further preclinical studies.
4. For the first time in Bulgaria, via the method of induced *in vitro* mutagenesis, mutant clones of reference strains *M. smegmatis* and *M. tuberculosis* H37Rv resistant to increasing concentrations above the established minimal inhibitory concentration of the selected compound were obtained. The identified mutation in gene Rv3755c is associated with drug resistance and drug tolerance.

VII. PUBLICATIONS RELATED TO THE DISSERTATION

1. Valcheva, V., Simeonova, R., Mileva, M., Philipov, S., Petrova, R., **Dimitrov, S.**, Georgieva, A., Tsvetanova, E., Teneva, Y. и Angelova, V.T**. (2022).** *In Vivo* Toxicity, Redox-Modulating Capacity and Intestinal Permeability of Novel Aroylhydrazone Derivatives as Anti-Tuberculosis Agents. *Pharmaceutics*, 15(1), 79.IF: 5,500,Q1

2. **Dimitrov, S**., Slavchev, I., Simeonova, R., Mileva, M., Pencheva, T., Philipov, S., Georgieva, A., Tsvetanova, E., Teneva, Y., Rimpova, N. and Dobrikov, G., **(2023)**. Evaluation of Acute and Sub-Acute Toxicity, Oxidative Stress and Molecular Docking of Two Nitrofuranyl Amides as Promising Anti-Tuberculosis Agents. *Biomolecules*, *13*(8), 1174, IF: 6.525, Q1
3. Мокроусов И.В., Ангелова В., **Димитров С.**, Чекрыгин С.А., Вылчева В.**, (2025)** Адаптация Mycobacterium tuberculosis к новому производному ароилгидразона *in vitro* и возможная роль гена Rv3755c. Бюллетень экспериментальной биологии и медицины, Том 179, № 4; IF: 0.9; Q3

VIII. CITATIONS NOTED

Article: Valcheva, V., Simeonova, R., Mileva, M., Philipov, S., Petrova, R., **Dimitrov, S**., Georgieva, A., Tsvetanova, E., Teneva, Y., & Angelova, V.T. (2022). *In Vivo* Toxicity, Redox-Modulating Capacity and Intestinal Permeability of Novel Aroylhydrazone Derivatives as Anti-Tuberculosis Agents. *Pharmaceutics*, 15(1), 79. IF: 5.500, Q1

Cited in:

1. Tafere, D.A., Gebrezgiabher, M., Elemo, F., Atisme, T.B., Ashebr, T.G., & Ahmed, I.N. (2025). Hydrazones, hydrazones-based coinage metal complexes, and their biological applications. *RSC Advances*, 15(8), 6191-6207.

Article: Dimitrov, S., Slavchev, I., Simeonova, R., Mileva, M., Pencheva, T., Philipov, S., Georgieva, A., Tsvetanova, E., Teneva, Y., Rimpova, N., & Dobrikov, G. (2023). Evaluation of Acute and Sub-Acute Toxicity, Oxidative Stress and Molecular Docking of Two Nitrofuranyl Amides as Promising Anti-Tuberculosis Agents. *Biomolecules*, 13(8), 1174. IF: 6.525, Q1

Cited in:

1. Berisio, R., & Ruggiero, A. (2023). Virulence Factors in Mycobacterium tuberculosis Infection: Structural and Functional Studies. *Biomolecules*, 13(8), 1201.
2. Gawad, J., Bonde, C., Bonde, S., Sharma, M., Suthar, D., Palkar, M., & Raghuwanshi, V. (2025). Investigating the Impact of Acute and 28-days Oral Exposure to Decaprenyl Phosphoryl-β-D-ribose 2'-epimerase (DprE1) Inhibitors on Vital Organ Function in Swiss Albino Mice. *Indian Journal of Pharmaceutical Education and Research*, 59(1s), s151-s158.

3. Nazeer, M., Shah, N., Ullah, S., Ikram, M., Amirzada, M.I., Alamoudi, A.J., Alshamrani, M., & Shah, A.J. (2025). Toxicological profiling and diuretic potential of arbutin via aldosterone synthase gene inhibition. *Life Sciences*, 123661.
4. Lafdil, F.Z., Nouioura, G., El Fadili, M., Lafdil, H., Mekhfi, H., Conte, R., Abuelizz, H.A., & Kandsi, F. (2025). LC-MS/MS Profiling and Toxicological Evaluation of Argania spinosa Extract: Acute and Subacute Studies in Swiss Albino Mice *with In Vivo* and In Silico Approaches. *Journal of Ethnopharmacology*, 120009.
5. da Silveira Gomes, R.N., da Conceição Veríssimo, J.D.F., dos Santos, I.P., da Rocha, M.H., Fontes, T.A., de Oliveira Dias, T., & dos Anjos, J.S.P. (2025). Adjuvant strategies in tuberculosis treatment: reducing oxidative stress and drug-induced neurotoxicity. *Journal of Media Critiques*, 11(27), e282-e282.

IX. PARTICIPATION IN SCIENTIFIC FORUMS

Oral Presentations:

Dimitrov, S., Valcheva, V. Broad biological screening of new chemical compounds as effective anti-tuberculosis drug candidates, Third Interdisciplinary Doctoral Forum, Kyustendil, June 6-7, 2022.

Dimitrov, S.; Slavchev, I.; Simeonova, R.; Mileva, M.; Pencheva, T.; Philipov, S.; Georgieva, A.; Tsvetanova, E.; Teneva, Y.; Rimpova, N.; Valcheva, V.; Dobrikov, G. Screening of novel nitrofuranyl amides for their *in vitro* antimycobacterial activity and *in vivo* evaluation of their pharmacological potential – Fourth Interdisciplinary Doctoral Forum, May 16-19, 2023, Sandanski.

Valcheva, V., Slavchev, I., **Dimitrov, S.,** Simeonova, R., Mileva, M., Georgieva, A., Tsvetanova, E., Pencheva, T., Dobrikov, G. Evaluation of acute and sub-acute toxicity, oxidative stress and molecular docking of two nitrofuranyl amides as promising anti-tuberculosis agents – 27th Congress of the Asian Pacific Society of Respirology (APSR 2023), November 16-19, 2023, Suntec City, Singapore.

Valcheva, V., **Dimitrov, S.,** Angelova, V., Mokrousov, I. Molecular insights into *Mycobacterium tuberculosis* resistance to novel aroylhydrazones revealed through *in vitro* mutagenesis and whole-genome sequencing. Presented at the World Conference on Lung Health, November 12-16, 2024, Bali, Indonesia.

Poster Presentations:

1. **Dimitrov, S.,** Simeonova, R., Mileva, M., Philipov, S., Valkova, I., Georgieva, A., Tsvetanova, E., Petrova, R., Angelova, V., Valcheva, V. *In vivo* toxicity, redox-

modulating capacity and intestinal permeability of novel aroylhydrazone derivatives with high *in vitro* antimycobacterial activity. MMCS2022 – Shaping Medicinal Chemistry for the New Decade, Rome, Italy, July 25-30, 2022.

2. **Dimitrov, S**., Simeonova, R., Mileva, M., Philipov, S., Valkova, I., Georgieva, A., Tsvetanova, E., Petrova, R., Angelova, V., Valcheva, V. *In vitro* and *in vivo* antimycobacterial activities of novel aroylhydrazone derivatives. EMBO, Tuberculosis 2022: From innovation to intervention, Paris, France, September 12-16, 2022.
3. **Dimitrov, S**., Angelova, V., Mokrousov, I., Valcheva, V. Spontaneous mutations conferring antibiotic resistance to new aroylhydrazones at a range of concentrations in *Mycobacterium tuberculosis*, ECMID 2024 (34th European Congress of Clinical Microbiology and Infectious Diseases), April 27-30, 2024, Barcelona, Spain.